Numerical analysis of multi-factors effects on the leakage and gas diffusion of gas drainage pipeline in underground coal mines

Cai, Jitao; Wu, Jiansong; Yuan, Shuaiqi; Liu, Zhe; Kong, Desheng

DOI
10.1016/j.psep.2021.05.017

Publication date
2021

Document Version
Accepted author manuscript

Published in
Process Safety and Environmental Protection

Citation (APA)
Cai, J., Wu, J., Yuan, S., Liu, Z., & Kong, D. (2021). Numerical analysis of multi-factors effects on the leakage and gas diffusion of gas drainage pipeline in underground coal mines. *Process Safety and Environmental Protection*, *151*, 166-181. https://doi.org/10.1016/j.psep.2021.05.017

Numerical analysis of multi-factors effects on the leakage and gas diffusion of gas drainage pipeline in underground coal mines

Jitao Cai[a], Jiansong Wu[a,]*, Shuaiqi Yuan[b], Zhe Liu[a], Desheng Kong[a]

[a] School of Emergency Management & Safety Engineering, China University of Mining and Technology, Beijing 100083, China;

[b] Safety and Security Science Group, Faculty of Technology, Policy and Management, TU Delft, Delft, The Netherlands

*Corresponding author: jiansongwu@hotmail.com

Abstract: Gas drainage system is a critical technique to prevent gas outbursts in the underground coal mine. The leakage of gas drainage pipelines can pose serious threats to the safety production of underground mining. In this paper, a multi-factors gas drainage pipeline leakage and diffusion (GDPLD) model is proposed based on the OpenFOAM platform, which can analyze the leakage and diffusion characteristics inside the pipelines. With field measurement data in a coal mine, the GDPLD model is verified with good practicability. Furthermore, scenario analysis in the context of different leak sizes, locations, and pipeline diameters is presented to evaluate the specific characteristics of gas leakage and diffusion inside the pipeline with negative pressure. The results showed that the leakage accident close to the pump station with a large leak size and small pipeline diameter usually represents the worst case, and when gas sensors are installed downstream of the leakage location, it is helpful to realize effective detection of the leakage accident. This study can help to improve the understanding of the leakage and diffusion characteristics of gas drainage pipelines and

provide technical supports for the monitoring system design of the gas drainage pipelines in underground coal mines.

Keywords

Underground coal mine; Gas drainage pipelines; Gas leakage and diffusion; Computational fluid dynamics; OpenFOAM

1. Introduction

As a kind of clean-burning resource, Coalbed methane (CBM) has great potential to make up for the shortage of conventional natural gas resources (Liu et al., 2020; Zheng et al., 2019; Moore et al., 2012). However, CBM emitted from coal seams or other methane-containing formations under the mining process have posed a serious threat to safety mining due to the gas explosion and outburst issues (Cao et al., 2019; Liu et al., 2020; Lu et al., 2019; Wang et al., 2018; Zhou et al., 2020). Meanwhile, CBM has a strong absorption capacity of infrared radiation, and thus causes CBM to be an extremely environment-harmful greenhouse gas that can speed up global warming (Fan et al., 2020; Zhou et al., 2014). To prevent and mitigate the gas emission disaster in coal mines and realize the rational exploitation and utilization of the CBM resources, the gas drainage system is widely used over the past few decades (Park & Liang, 2016). As the main equipment for the transmission of the extracted gas resources, gas drainage pipelines usually suffer long-term exposure to the complex and harsh environment in the underground coal mine. Therefore, there is a great possibility of leakage accidents in the gas drainage pipeline induced by corrosions and man-made damages. Such accidents can debase the quality of the extracted gas and change the manner we treat

CBM from high-quality energy resources to hazardous gas (Zhou et al. 2014; Cheng et al., 2017; Zhao et al., 2018). Besides, subject to disaster-causing factors such as flame and electrostatic spark, gas-involved accidents including gas combustion or explosion might arise, which results in damage to the excavations, equipment, and casualties that cannot be predicted (Liu et al., 2020). Therefore, the leakage and diffusion characteristics of the gas drainage system should be seriously focused on. It plays a pivotal role in the enhancement of gas extraction efficiency and contributes to the safe operation of gas drainage and transportation in the underground coal mine.

There have been extensive studies conducted by using the numerical models to investigate the leakage characteristics around the borehole of the gas drainage system in underground coal mines (Liu et al., 2020a; Liu et al., 2020b; Zheng et al., 2017; Zhang et al., 2020; Fan et al., 2020; Wang et al., 2019; Zheng et al., 2016; Wang et al., 2019; Kang et al., 2018; Zhang et al., 2018). Liu et al. (2020a) compared two distinct theoretical models with the consideration of air leakage around the borehole in the coal seam. The results indicated that the C-model taking air leakage into account could reproduce a more reliable gas drainage process. Liu et al. (2020b) revealed the air leakage characteristics by developing a fully coupled gas flow model. It was found that a longer sealing length could increase the extracted gas concentration. Moreover, the air leakage induced by mining disturbance and the existence of fractures could be addressed by the novel sealing method, which integrates cement grouting and gel injection. Aim to investigate the effects of the coal properties on air leakage, Zheng et al. (2017) introduced the orthogonal design method and F-test theory integrated

approach. The results showed that Young's modulus had a significant role in the air leakage phenomenon compared with Poisson's ratio and Porosity. Based on the theoretical integration of air-methane mixing flow in fracture, matrix methane flow, mass transfer, and dynamic permeability, Fan et al. (2020) studied the air leakage numerically by developing a coupled compositional flow model. The simulation results demonstrated that higher pressure, longer sealing length, and the increase of sealing area were helpful to the drained gas concentration. Zhang et al. (2020) proposed an air-leakage model to investigate the different leakage patterns and thus served as a reference for the optimization of borehole-sealing techniques, which achieved a higher gas extraction concentration compared to the traditional sealing technique. Similarly, Wang et al. (2019) developed a coupled model taking coal deformation and air-CH_4 flow into account to describe the air leakage behaviors under different contributing factors. It showed that air leakage would decrease with an increase of active support pressure and an active support sealing method was proposed to realize higher extraction efficiency. Likewise, some researches (Kang et al., 2018; Liu et al., 2021; Zheng et al., 2016; Wang et al., 2019; Wang et al., 2020; Zhang et al., 2018; Zhang et al., 2020) have been conducted to provide practical guidance for air leakage prevention strategies around the borehole. However, these studies mentioned above mainly focused on air leakage behavior around boreholes of the gas drainage systems. The gas drainage pipeline that extends for thousands of meters is not investigated enough, especially the leakage and diffusion characteristics inside gas drainage pipelines are still not well understood.

In the past decades, different leakage scenarios of gas pipelines have been widely studied, such as the leakages of above-ground and buried pipelines (Okamoto and Gomi, 2011; Yan et al. 2015; Ebrahimi-Moghadam et al., 2016; Ebrahimi-Moghadam et al., 2018; Bezaatpour et al., 2020), gas leakage in the confined space (Wang et al., 2020; Zhang and Lan., 2020) and open space (Zhang et al., 2014; Zhang et al., 2015). However, the leakage of gas drainage pipelines in coal mine performs with different characteristics compared with the abovementioned leakage scenario. Firstly, the gas drainage pipeline is characterized by negative pressure, and thus sucks the external gas into the pipeline instead of forming a jet flow toward the ambient environment. Secondly, the pressure inside the gas drainage pipeline varies with different locations, causing location-related leakage behavior. Therefore, it is highly significant to investigate the leakage characteristics of the gas drainage pipeline.

In this study, a gas drainage pipeline leakage and diffusion (GDPLD) model was proposed to simulate the leakage and diffusion behaviors of the gas drainage pipeline based on the OpenFOAM platform. Firstly, the GPDLD model was developed according to the gas drainage system of a coal mine, located in Shanxi Province, China. Then, the proposed model was verified by empirical formula and the field measurement data. Furthermore, with the consideration of the main contributing factors (i.e. leak size, leak location, and pipeline diameter), different gas pipeline leakage scenarios were simulated to analyze the specific characteristics of the gas leakage and diffusion in gas drainage pipelines. Additionally, the alarm time of gas sensors was also investigated to provide a technical reference for the optimization of the monitoring system in

underground coal mines.

2. Methodology

2.1 Governing equation

To accurately capture the leakage and diffusion behavior of gas drainage pipelines in the underground coal mine, the continuity equation, momentum equation, and energy equation are involved in the proposed GDPLD model. Meanwhile, the no-reaction species transport equation and gas state equation are also considered to simulate the transportation of multi-component mixed gas. The mathematical equations mentioned above are listed as follows:

(i) Continuity equation

$$\frac{\partial \rho}{\partial t} + \nabla \cdot (\rho \mathbf{u}) = 0 \tag{1}$$

(ii) Momentum equation

$$\frac{\partial (\rho u)}{\partial t} + \nabla \cdot (\rho u \mathbf{u}) = -\frac{\partial p}{\partial x} + \nabla \cdot (\mu \nabla u) + F_x \tag{2}$$

$$\frac{\partial (\rho v)}{\partial t} + \nabla \cdot (\rho v \mathbf{u}) = -\frac{\partial p}{\partial y} + \nabla \cdot (\mu \nabla v) + F_y \tag{3}$$

$$\frac{\partial (\rho w)}{\partial t} + \nabla \cdot (\rho w \mathbf{u}) = -\frac{\partial p}{\partial z} + \nabla \cdot (\mu \nabla w) + F_z \tag{4}$$

(iii) Energy equation

$$\frac{\partial (\rho i)}{\partial t} + \nabla \cdot (\rho i \mathbf{u}) = -p \nabla \cdot \mathbf{u} + \nabla \cdot (k \nabla T) + \Phi + S_h \tag{5}$$

(iv) No-reaction species transport equation

$$\frac{\partial}{\partial \mathrm{t}} (\rho C_i) + \nabla \cdot (\rho C_i \mathbf{u}) = \nabla \cdot (D_c \nabla C_i) + S_i \tag{6}$$

(v) Gas state equation

$$pV = nZRT \tag{7}$$

Where ρ is the mixture density of multi-component gas including N_2, O_2, and

CH_4. $\mathbf{u}$ is the gas velocity and u, v, w denote normal velocity corresponding to x, y, z directions respectively. p represents the static pressure, i is the internal thermal energy and T is the thermodynamic temperature. Φ represents the dissipation function. C_i means gas volume fraction of every single gas involved in mixture gas, taking a mixture gas with n species for example, there are only n-1 species that need to be specified since the sum of n species is equal to unity. F_x, F_y and F_z are the momentum source term related to the body force. S_h and S_i are source terms accounting for the internal heat source and mass source. μ, k, and D_c are physical parameters associated with internal friction, heat transfer, and diffusion capacity respectively. V, n, Z, and R involved in the state equation represent gas volume, amount of substance, compressibility, and the gas constant.

2.2 Turbulence model

Thanks to the low-cost requirement of computing resources and wide range of applicability, the standard k-ε model has gained much attention and adoptions in the last few decades (Wang et al., 2020). However, the standard k-ε model has trouble in handling fluid adjacent to walls and thus yields unreliable results (Sklavounos and Rigas, 2004). Therefore, the SST model was developed in response to the shortages of the k-ε model and could give better performance in the near-wall simulations (Mentor, 1994; Mentor, 2003), which was applied for the simulation of turbulence flow in this study. The mathematical equations of the SST model are presented as follows:

$$\frac{\partial(\rho k)}{\partial t} + \nabla \cdot (\rho k \mathbf{u}) = \nabla \cdot ((\mu + \sigma_k \mu_t) \nabla k) + P - \rho \beta^* \omega k \tag{8}$$

$$\frac{\partial(\rho \omega)}{\partial t} + \nabla (\rho \omega \mathbf{u}) = \nabla \cdot ((\mu + \sigma_\omega \mu_t) \nabla \omega) + \frac{\gamma}{\nu_t} P - \rho \beta \omega^2 \tag{9}$$

$$+2(1-F_1)\frac{\rho\sigma_{\omega 2}}{\omega}\nabla k\nabla\omega$$

Where k is turbulence kinetic energy, ω represents the turbulence dissipation rate. P and μ_t are the production rate of turbulence and turbulence viscosity. SST model combines the advantage of k-ε and k-ω model by computing a blend function F_1, which is equal to 0 far away from the near-wall area and switches to 1 at the boundary layer. The specific configuration parameters of the SST model are listed in Table A1 according to Mentor's research (Mentor, 2003).

2.3 PIMPLE algorithm

As a fast-growing open-source computing platform using the finite volume method (FVM), OpenFOAM is characterized by high extensibility and good accuracy (Mack and Spruijt, 2013; Tran et al., 2020). Meanwhile, it has been verified that OpenFOAM has great potentials in the simulation of heavy gas leakage and multi-component gas transportation scenarios (Fiates and Vianna, 2016). To realize the numerical simulation of gas pipeline leakage in underground coal mines, the gas drainage pipeline leakage and diffusion (GDPLD) model was developed based on the OpenFOAM platform. Generally, the pressure-velocity coupling scheme is an extremely time-consuming work due to the multi-iteration pressure correction algorithm. When coping with a large computational domain like the gas drainage pipeline, this problem becomes more serious. The Pressure Implicit Method for Pressure Linked Equations (PIMPLE) algorithm can take responsibility to solve the pressure-velocity coupling scheme with good stability in dealing with large time steps, which is appropriate for handling the problem mentioned above. The specific process

of the PIMPLE algorithm is presented in Fig. 1.

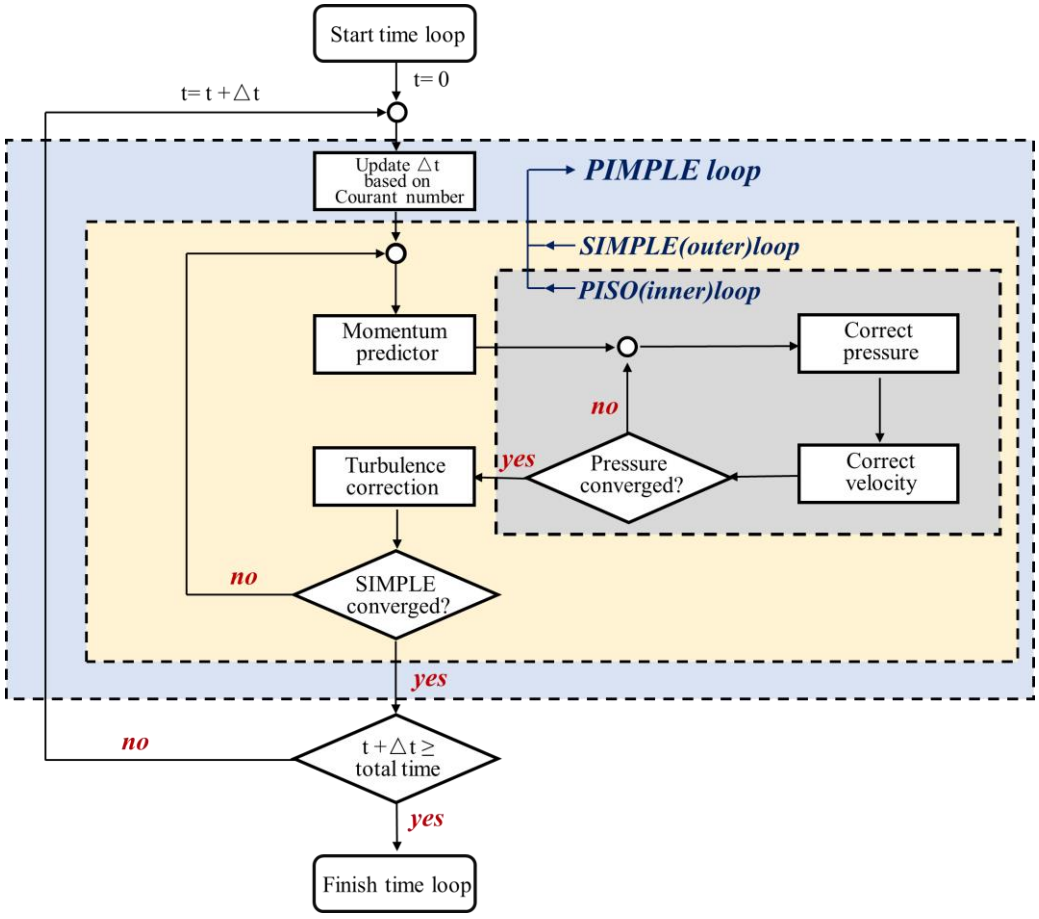

Fig. 1 Process of PIMPLE algorithm.

As shown in Fig. 1, the PIMPLE algorithm performs as a combination of the Semi-Implicit Method for Pressure Linked Equations (SIMPLE) and Pressure Implicit with Splitting of Operators (PISO) algorithm. For the inner loop, a conventional PISO algorithm is employed to calculate pressure correction with a limited number of iterations. For the outer loop, absolute tolerance and iteration number are considered as the convergence criteria, which makes the calculation go fast when the solution is stable but can also give room for multi-iterations when instability occurs. Overall, the PIMPLE algorithm offers good flexibility for a large time step and guarantees the stability of the calculation, which serves as an ideal choice in the development of the GDPLD model.

3. Results and discussion

3.1 Validation of GDPLD model

In this section, the proposed GDPLD model is evaluated by using an empirical formula in a previous study and the field monitoring data from a coal mine. The whole gas drainage system of the investigated coal mine is shown in Fig. 2. Methane contained in the coal seam, regardless of either free state or adsorbed state, is extracted into the gas drainage pipeline under negative pressure provided by the pump station, and then can be transported to the ground system for further utilization (Zhou et al. 2014). In this study, only the gas drainage pipelines were taken into account and set as the computational domain. As the gas extraction work proceeds, there will be a relatively stable flow field in the borehole zone and the gas drainage pipeline (Peng et al., 2015; Liu et al., 2020; Fan et al., 2020). Therefore, some key parameters used in the boundaries of the gas drainage pipelines, such as pressure and gas concentration, can be obtained from the field monitoring data or empirical determination. The parameters configuration and the verification process are presented in the following section.

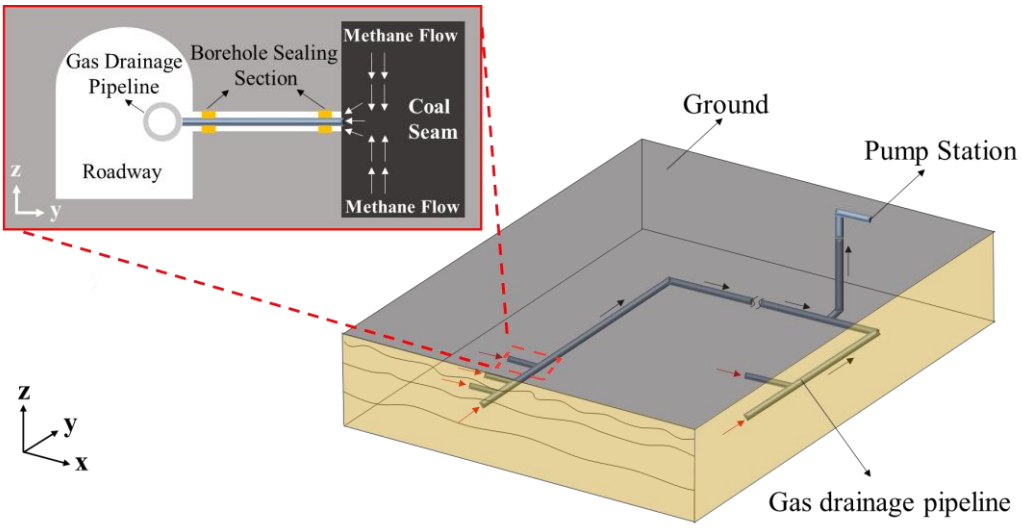

Fig. 2 Schematic of gas drainage process.

3.1.1 Numerical configurations

The computational domain used in this study consists of the pipelines with three different diameters (426mm, 630mm, 820mm), which is illustrated in Fig. 3. Moreover, Fig. 3 presents the layout and boundaries of the gas drainage pipeline. The configuration parameters of the gas drainage pipelines are provided in Table A2.

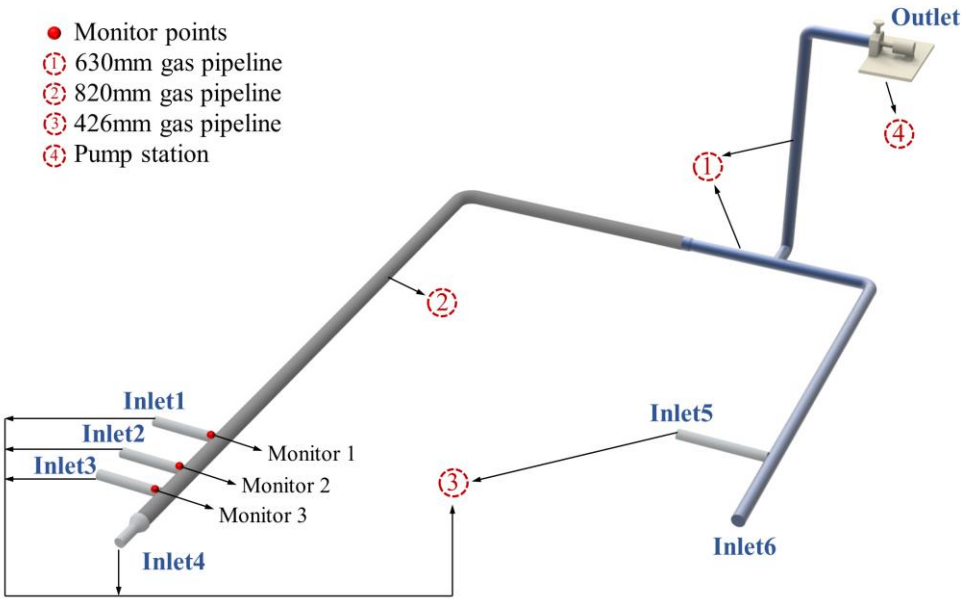

Fig. 3 Computational domain of the gas drainage pipeline model.

Since the gas flow in the gas drainage pipelines is driven by pressure, a total pressure inlet and static pressure outlet coupling scheme are adopted for the numerical simulation. The walls of the gas drainage pipelines are regarded as a rough wall with a 0.01 m roughness height considering the corrosion, obstacle, and accumulated water in the gas drainage pipelines. Finally, the specific parameters related to boundary conditions obtained from field monitoring data are concluded in Table 3.

Table 3 Boundary condition parameters

Region	Boundary conditions	Value
Inlet1	Total pressure (Pa)	81205
	Temperature (K)	289.96
Inlet2	Total pressure (Pa)	81415
	Temperature (K)	293.78
Inlet3	Total pressure (Pa)	81525
	Temperature (K)	291.34
Inlet4	Total pressure (Pa)	82825
	Temperature (K)	294.84
Inlet5	Total pressure (Pa)	83035
	Temperature (K)	290.86
Inlet6	Total pressure (Pa)	84805
	Temperature (K)	293.28
Outlet	Static pressure (Pa)	65445
	Temperature (K)	287.15

In this paper, mesh independence analysis is also investigated to ensures reliable numerical solutions. The computational domain is created and discretized by Ansys ICEM-CFD. Owing to the irregular shape of the local elements installed in gas drainage pipelines like elbow and T-pipe, there is a crux in discretizing the computational domain using hexahedral cells only. However, if the automatic tetrahedral cell scheme is adopted, the computational intensity will be extremely increased due to tremendous tetrahedral cells existing in the computational domain. Therefore, the hybrid mesh technique integrating hexahedral and tetrahedral cells is utilized with both geometric adaptability and computing efficiency, which is shown in Fig. 4. After the discretization of the computational domain, four kinds of mesh with different grid numbers are employed for mesh independence analysis.

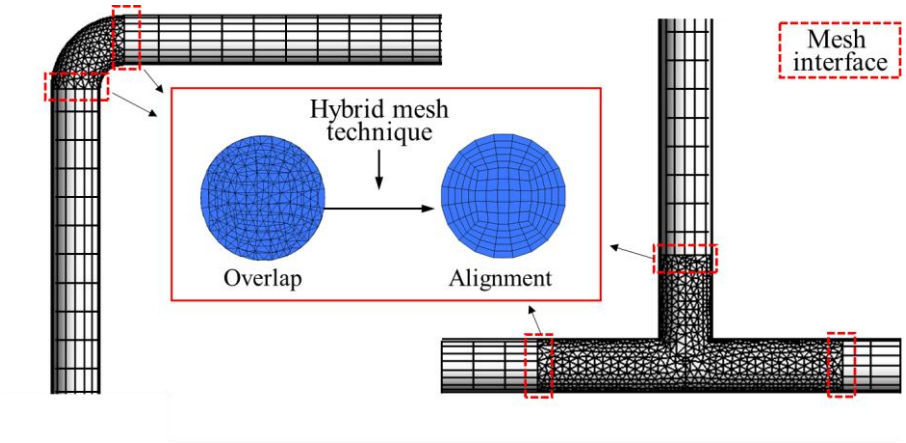

Fig. 4 Schematic of hybrid mesh technique.

The comparison of simulation results obtained from four different mesh cases with grid numbers of 160 thousand, 260 thousand, 360 thousand, and 520 thousand is shown in Fig. 5. As seen from Fig. 5, the max relative error and average relative error between Mesh1 and Mesh2 are 10.22% and 1.86%. As the stepwise refinement of grids, there is a negligible difference between Mesh_3 and Mesh_4 (the max relative error and average relative error are 1.68% and 0.27% respectively). Therefore, Mesh_3 is selected as a suitable mesh for the following simulation and analysis with the consideration of both computational accuracy and efficiency.

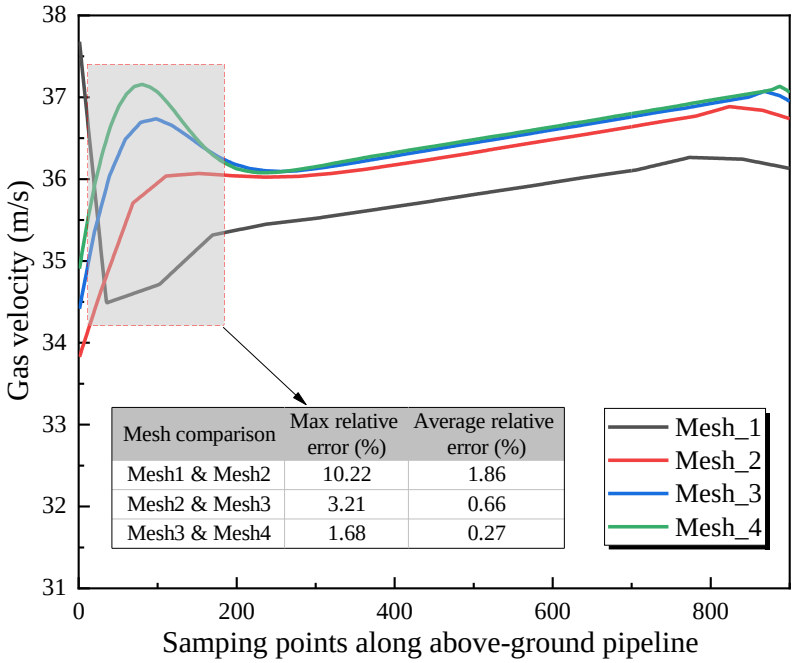

Mesh comparison	Max relative error (%)	Average relative error (%)
Mesh1 & Mesh2	10.22	1.86
Mesh2 & Mesh3	3.21	0.66
Mesh3 & Mesh4	1.68	0.27

Fig. 5 Mesh independence analysis.

3.1.2 Results analysis

Generally, there is an initial region characterized by progressive acceleration when coping with pipe and duct flow near the entrance (Anselmet et al., 2009). This is because the progressive thickening of the boundary layer results in a decrease of pipeline cross-section. According to the research of Anselmet, the length of the initial region can be calculated by the formula (10) as follows:

$$Le = 2D \cdot Re^{0.25} \tag{10}$$

Where Le is the length of the initial region. D and Re represent the hydraulic diameter and Reynolds number respectively.

Firstly, the specific flow characteristic of the pipeline mentioned above is utilized to evaluate the GDPLD model. After the simulation reaches a relatively steady state, the velocity profile along the pipeline is extracted and plotted in Fig. 6. It shows a gradual acceleration behavior at the entrance of the gas drainage pipeline, and then the

full development of gas flow is reached as gas moves away from the entrance, which can be seen in Anselmet's study similarly. Secondly, to avoid the influence of disturbing flow, the results calculated by the formula (10) at the location of Inlet4 and Inlet6 are listed in Table 4 for further quantitative comparison. Table 4 shows that there is a subtle error observed in the case of Inlet4. The reason for this may be that the existence of pipeline diameter transition causes small disturbances. However, a high agreement between the results calculated from formula (10) and the simulation results is obtained in Table 4, which indicates the proposed model has good practicability in simulating the flow characteristics of gas drainage pipelines.

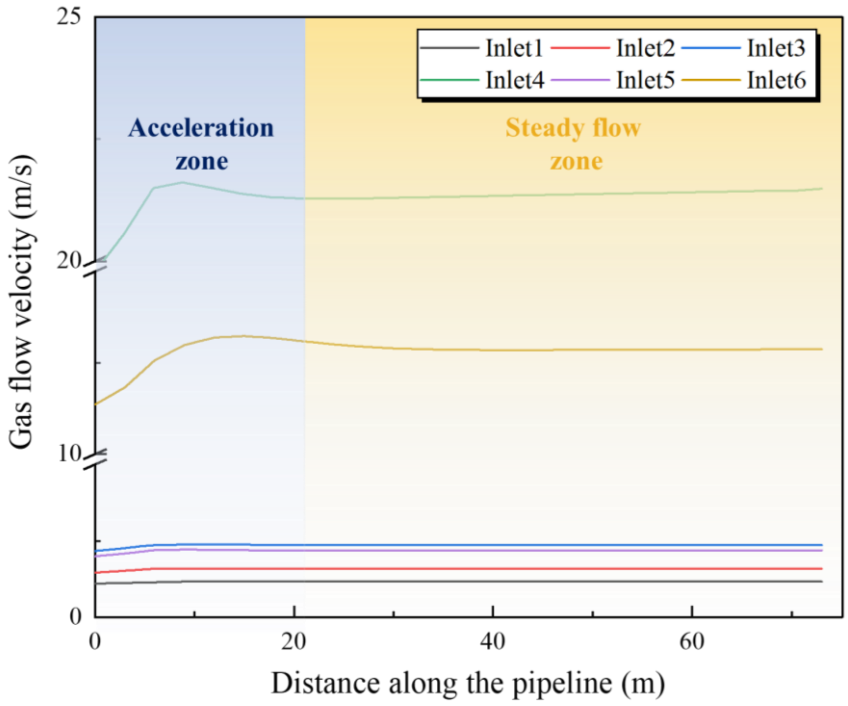

Fig. 6 Velocity profile of Inlet region.

Table 4 Results comparison of *Le* between empirical formula and simulation

Initial region	Velocity range (m/s)	Hydraulic diameter (m)	Formula results	Simulation results
Inlet 4	19.78~21.61	0.426	25.81~26.39	24.69
Inlet 6	11.35~13.23	0.630	36.64~38.07	37.68

Furthermore, the comparison between the simulation results and the field

monitoring data is presented in Table 3. P_1, P_2, and P_3 denote the pressure in the location depicted in Fig. 3 in the form of the red dot. Q is the volumetric flow rate near the location of the pump station. As shown in Table 5, the relative errors between the simulation results and the field monitoring data are all within the range from 0.58% to 4.30%, which can be regarded as an acceptable and reasonable result. The proposed GPDLD model is capable of reproducing the gas flow characteristics and gas drainage process in the gas drainage pipelines. Therefore, it can be used for the following analysis.

Table 5 Results comparison of GPDLD model and field monitoring data

Data results	P_1(Pa)	P_2(Pa)	P_3(Pa)	Q(m^3/min)
GPDL model	81202	81404	81490	518.38
Field data	80735	78965	79305	497
Relative error (%)	0.58	3.09	2.76	4.30

3.2 Effects of multi-factors on gas pipeline leakage and diffusion

The size of the leak hole, the pressure difference at the leakage location, and the diameter of the pipeline are of significance in influencing the severity of the leakage consequence (Ebrahimi-Moghadam et al., 2018; Wang et al., 2020). Therefore, with the consideration of these three contributing factors, a gas drainage pipeline model is developed to investigate the leakage and diffusion characteristics when an unexpected leakage occurs. Meanwhile, the quantitative analysis of the leakage volumetric flow rate and the alarm time of gas sensors are involved as well.

3.2.1 Numerical configurations

Similarly, the computational domain is constructed and discretized in the same

way as mentioned in Section 3.1.1. Compared with the physical model built in Section 3.1.1, the physical model investigated in this section only includes the portion of the gas drainage pipeline. The geometric layout and boundary conditions are shown in Fig. 7. Moreover, the configuration parameters of the computational domain related to different leakage scenarios are detailed in Table 6.

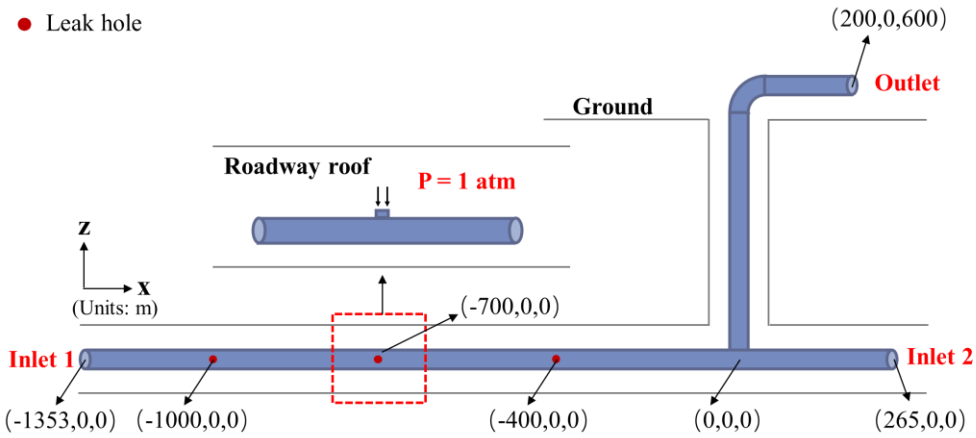

Fig. 7 Computational domain of the partial gas drainage pipeline model.

Table 6 Parameters of different simulation scenarios

	Scenario	Leak diameter (mm)	Pipeline diameter (mm)	Leak location (m)
Leak sizes	Case 1	100	820	(-700,0,0)
	Case 2	200	820	(-700,0,0)
	Case 3	300	820	(-700,0,0)
Leak locations	Case 4	200	820	(-700,0,0)
	Case 5	200	820	(0,0,300)
	Case 6	200	820	(100,0,600)
Pipeline diameters	Case 7	200	426	(-700,0,0)
	Case 8	200	630	(-700,0,0)
	Case 9	200	820	(-700,0,0)

According to the installation requirement of the KJ370 pipeline monitoring system, 10 methane sensors are assumed on both sides of the leak location every 10 meters symmetrically (approximately equal to 13 times of pipe diameter). Meanwhile, the leak location is assumed to be in the middle of the two gas sensors as the worst leakage scenario. The locations of gas sensors are listed in Table 7.

Table 7 Relative location of gas sensors ("0" represents the leak location)

Sensor index	0	1	2	3	4	5	6	7	8	9	10
X coordinate (m)	0	5	15	25	35	45	-5	-15	-25	-35	-45

The specific boundary conditions used in this section are shown as follows:

(1) Inlet1 & Inlet2: The total pressure boundary conditions are employed with P_{Inlet1}=79835 Pa and P_{Inlet2}=79805 Pa, which are extracted from the verified case in Section 3.1 at the corresponding location.

(2) Outlet: The pressure at Outlet is set as 65445 Pa with a static pressure condition.

(3) Leakage: The leak hole is defined as total pressure conditions with P_{Leak}=101325Pa, which is the atmospheric pressure.

Finally, the initial gas concentration is set as 25% VOL referring to the average gas drainage concentration in China (Wang et al., 2016). And the steady flow field without leakage will be computed in advance and perform as the initial condition for the leakage scenarios.

3.2.2 Effects of leak sizes

Three leakage scenarios of different leak sizes with constant leak location and pipeline diameter are simulated and analyzed (i.e., Case 1, Case 2, and Case 3 in Table 6). As seen from Fig. 8, the high-velocity area is formed near the leak location due to the large pressure difference between the gas drainage pipeline and the external space. It can be seen that the high-velocity area increases with the increase of leak size. When the leak size is 100 mm, the high-velocity area is small and cannot reach the bottom of the gas drainage pipeline. However, this phenomenon is not obvious in the case of 200 mm and 300 mm. The reason may be because the leakage gas flow of small leak size is

relatively unstable, and thus easier to be influenced by the mainstream inside the gas drainage pipeline.

Moreover, the leakage scenario of various leak sizes has a direct impact on the leakage volumetric flow rate, which can be observed in Fig. 9. The leakage volumetric flow rate of all three cases has a downward trend over time due to the decreasing pressure gradient between the leak hole and the internal flow field. Furthermore, the Relative variation ratio (RVR) is used to measure the change of leakage flow rate over time.

$$RVR = \frac{E - S}{S} \tag{51}$$

Where the RVR means a relative error of the leakage flow rate, S (Starting) and E (Ending) represent the leakage flow rate at the beginning and the end of the pipeline leakage respectively.

Fig. 9 shows that the RVR has a growing trend with the increase of leak size. This may be because the bigger the leak size is, the easier the leakage will affect the gas flow inside the gas drainage pipeline, and thus the faster the pressure gradient decreases. The maximum leakage volumetric flow rate increases significantly with the increase of leak size, which aggravates the severity of the leakage consequence. Therefore, the leakage scenario with a large leak size will produce a large leakage gas flow and volumetric flow rate, which seriously affects the gas drainage process.

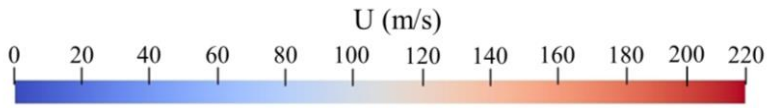

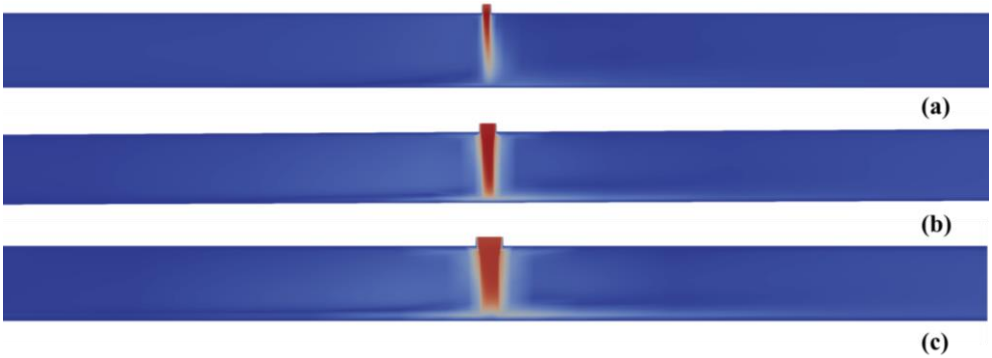

Fig. 8 Velocity contour of different leak sizes, (a) Case 1: 100mm, (b) Case 2: 200mm, (c) Case 3: 300mm.

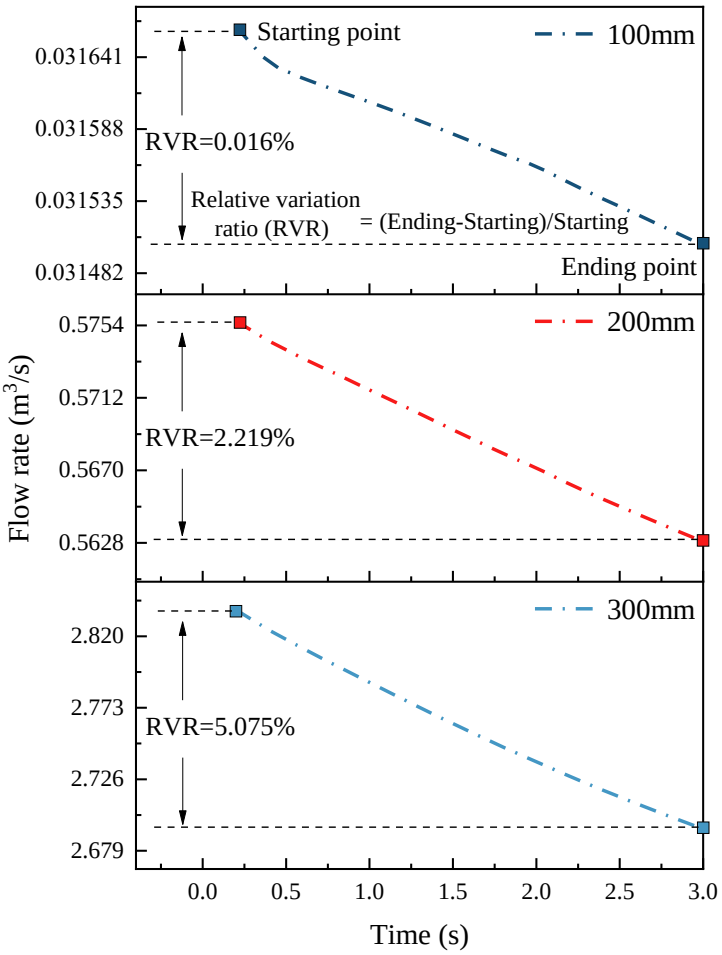

Fig. 9 Effect of different leak sizes on leakage volumetric flow rate.

In this paper, the process of gas diffusion inside the gas drainage pipelines can be divided into two stages according to the different diffusion characteristics, namely, vortex flow (dominated by vortex generated near the leak location) and fully-developed flow (dominated by velocity profile of fully-developed pipeline flow). The contour of

the CH4 concentration corresponding to the different diffusion stages is shown in Fig. 10. When the leak size is 100 mm and the leak time is 0.2 s, the diffusion range of the lower part of the pipeline is larger than that of the upper part. This is because the gas flow inside the pipeline is dominated by the vortex flow downstream of the leak location at the beginning of the leakage. From 0.8 s to 1 s, the flow stage changes from vortex flow to fully-developed flow, which is a relatively stable diffusion process. By comparison, when the leak sizes are 200 mm and 300 mm, it only needs 0.6 s and 0.4 s to reach the fully-developed flow. Meanwhile, the low concentration area affected by the leakage accident is larger. It should be noted that the influenced region upstream of the leak location is relatively small. This is because the mainstream inside the gas drainage pipeline prevents reverse diffusion to a large extent. The largest influence region can be observed when the leak size is 300 mm, which demonstrates the relatively bad effect of a large leak size.

Furthermore, in order to analyze the spatial and temporal distribution of CH4 concentration quantitatively. The volume fraction of CH4 at the specific sampling points corresponding to the gas sensors layout mentioned in the previous section is plotted in Fig. 11 and Fig. 12. Except for explosion limits for methane (0.05-0.16 VOL), the alarm threshold is assumed to 0.2 VOL by referring to the difference between the lower explosive limit and the alarm concentration of methane (0.01 VOL and 0.05 VOL) (Wang et al., 2020; Zhang and Lan, 2020). Firstly, the gas concentration of sensor 1 and sensor 6 that are closest to the leak location is presented in Fig. 11. As shown in Fig. 11 (a), the CH4 concentration has a decreasing trend at the initial stage and then retains a

constant value as time goes on. The alarm times for three cases are 0.77s, 0.32s, and 0.19s respectively due to the different leakage volumetric flow rates. Meanwhile, the larger the leak size is, the faster the CH4 concentration decreases. However, it should be aware that although a large leak size can cause an extremely low CH4 concentration, which significantly affects the quality of extracted gas. A dangerous CH4 concentration range may be sustained for a long time when the leak size is relatively small (200mm in this study), which poses a potential threat of gas fire and explosion. As seen from Fig. 11(b), when the leak size is 100mm, the concentration variation cannot be captured by senor 6 compared with the case of 200mm and 300mm. This is because sensor 6 is located upstream of the leakage location and thus inevitably influenced by the mainstream. Fig. 12 shows the concentration variation of all gas sensors used in this study. It can also be obtained that the gas sensors downstream of the leak location have a shorter alarm time compared with the gas sensors located upstream in the symmetrical location. Therefore, the gas sensors distributed downstream of the leak location can capture the leakage accident more effectively, especially for a large leak size.

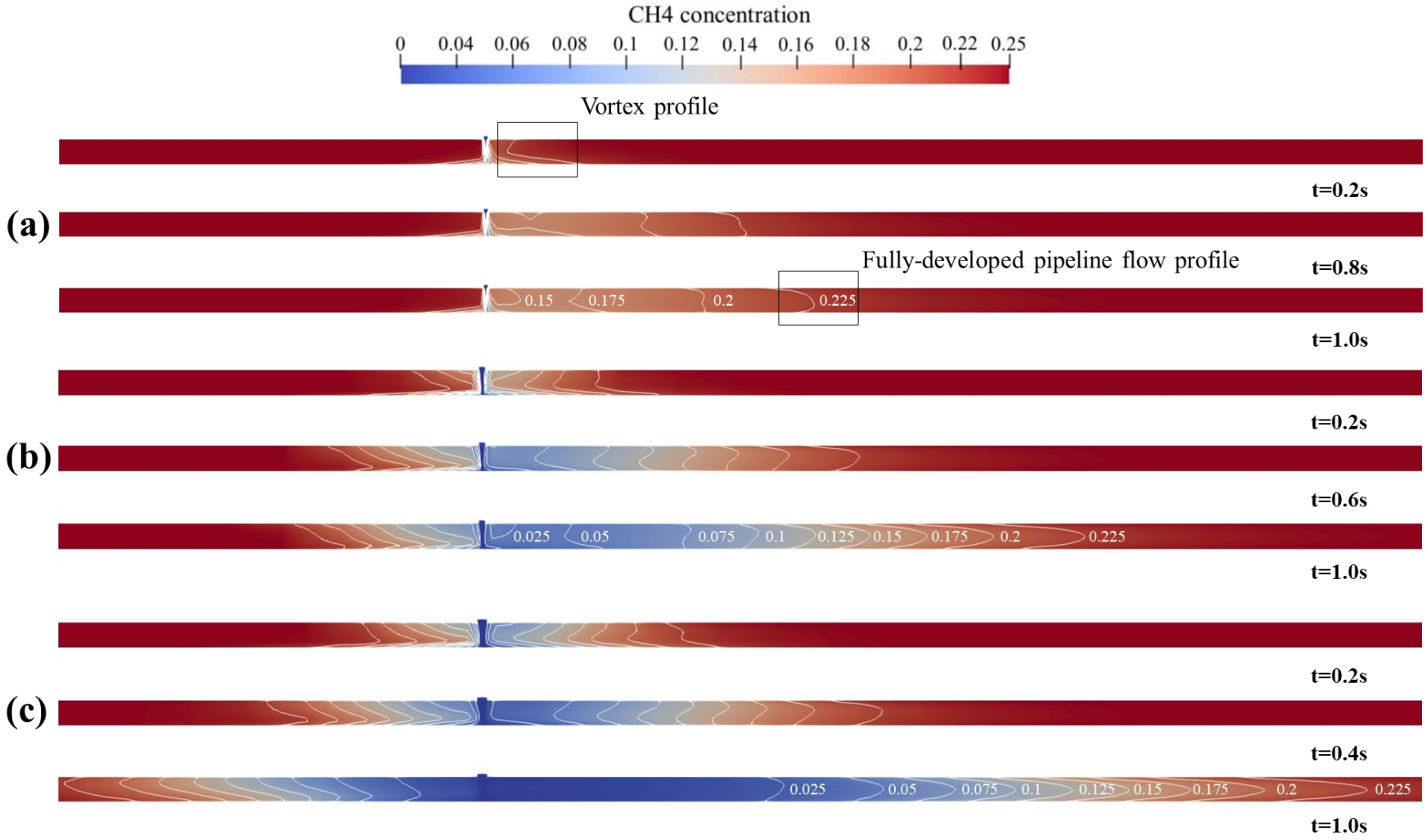

Fig. 10 CH4 concentration distribution of different leak sizes, (a) Case 1: 100mm, (b) Case 2: 200mm, (c) Case 3: 300mm.

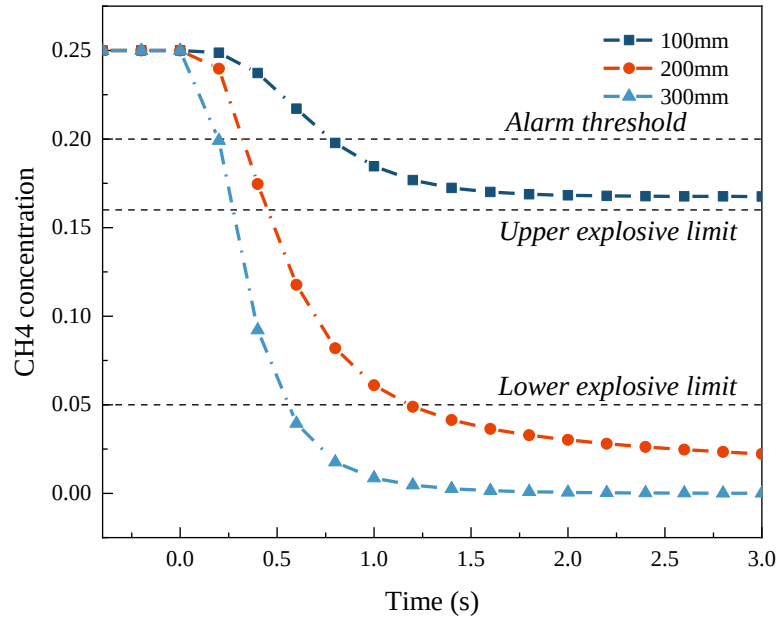

(a)

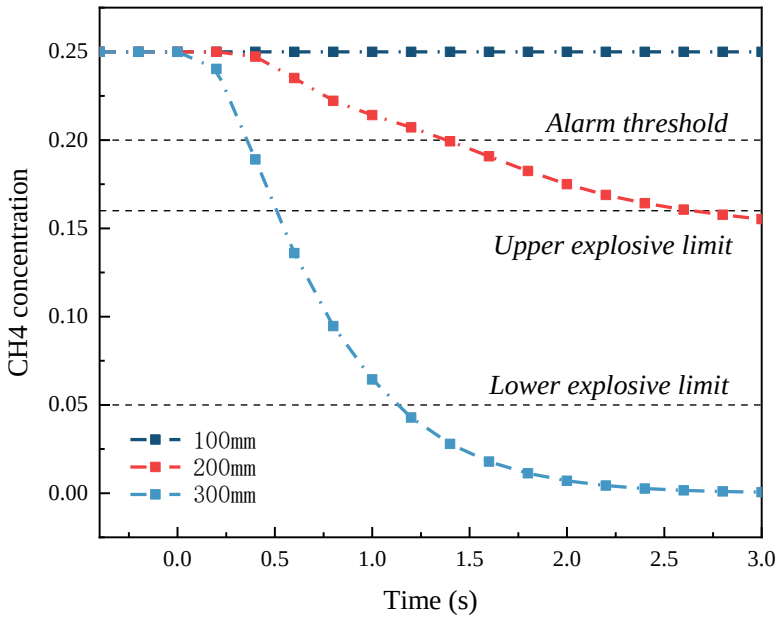

(b)

Fig. 11 Effect of different leak sizes on alarm time, (a) sensor 1,(b) sensor 6.

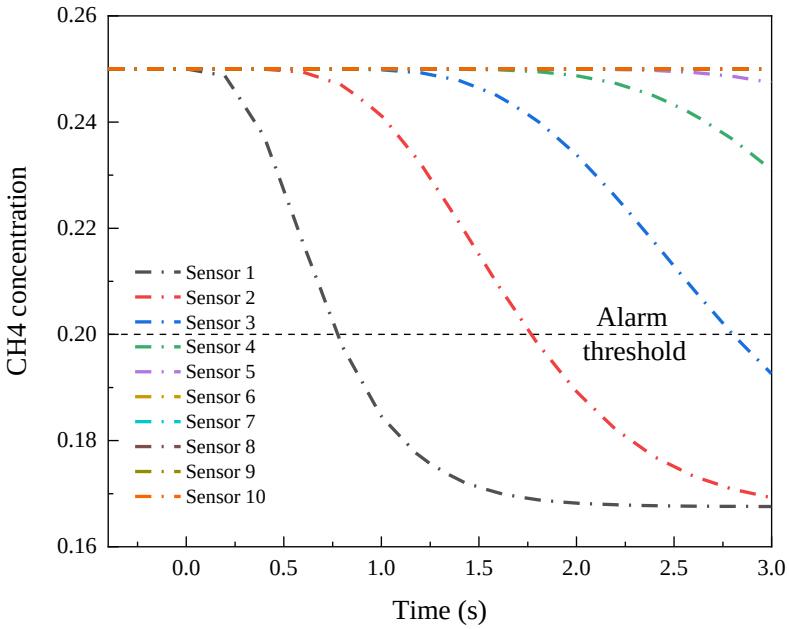
CH4 concentration
Time (s)
Alarm
threshold
Sensor 1
Sensor 2
Sensor 3
Sensor 4
Sensor 5
Sensor 6
Sensor 7
Sensor 8
Sensor 9
Sensor 10

(a)

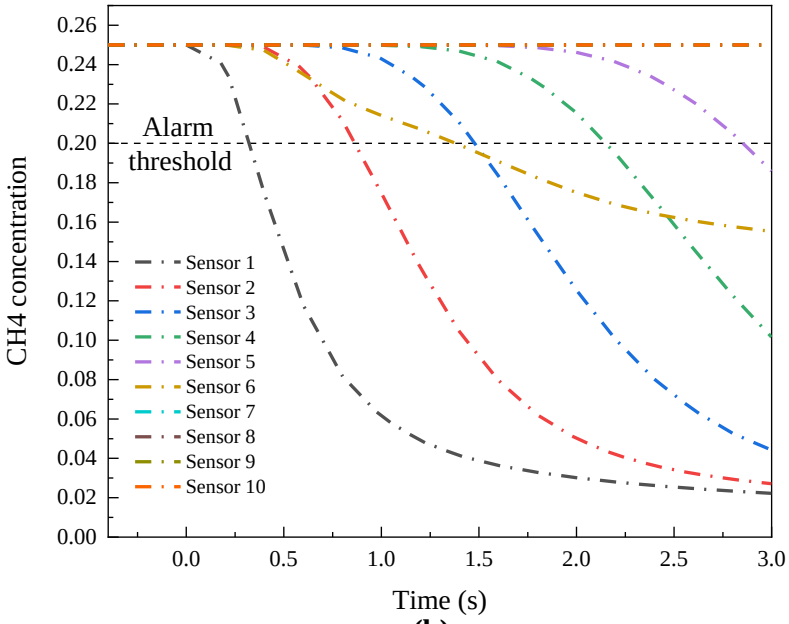
CH4 concentration
Time (s)
Alarm
threshold
Sensor 1
Sensor 2
Sensor 3
Sensor 4
Sensor 5
Sensor 6
Sensor 7
Sensor 8
Sensor 9
Sensor 10

(b)

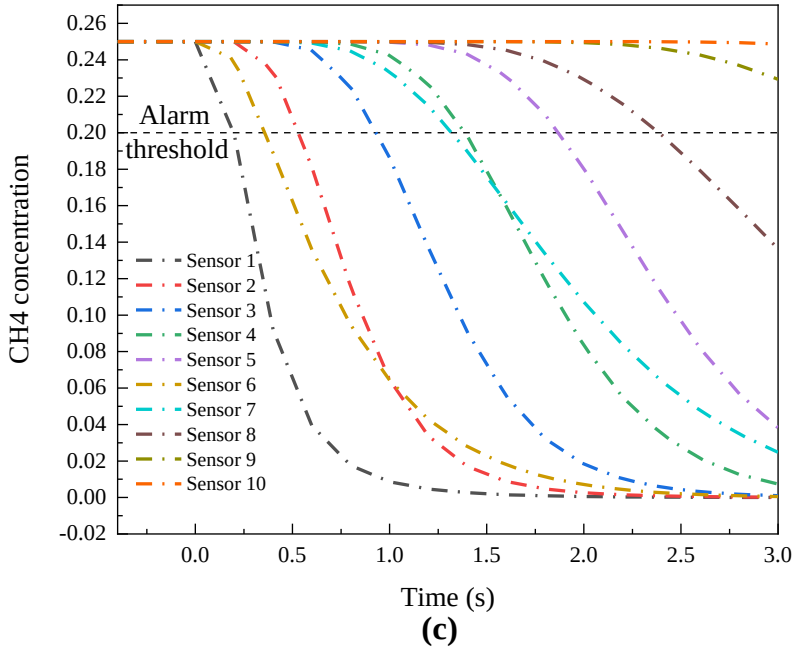

(c)

Fig. 12 Effect of different leak sizes on alarm time, (a) Case 1: 100mm, (b) Case 2: 200mm, (c) Case 3: 300mm.

3.2.3 Effects of leak locations

With the consideration of the distance from the pump station, three different leak locations (underground pipeline, vertical pipeline, and above-ground pipeline, i.e., Case 4, Case 5, and Case 6 in Table 6) are regarded as the leak locations. Fig. 13 presents the variation of gas velocity contour with different leak locations. By comparing with the case of underground pipeline leakage, the velocity contour in the cases of vertical pipeline and above-ground pipeline leakage has a slight deviation in the lower part of the pipeline at the leak location. This may be because that an acceleration area will be formed at the vertical pipeline due to the energy conversion between kinetic energy, pressure potential energy, and gravity potential energy, which results in a relatively

strong mainstream at vertical and above-ground pipeline. The velocity range inside the gas drainage pipeline at different locations (i.e., underground pipeline, vertical pipeline, above-ground pipeline) is presented in Table 8 to validate the assumption mentioned above. It can be seen that the closer to the pump station, the larger the velocity magnitude of the mainstream, and thus the greater impact on the leakage gas flow.

As can be seen from Fig. 14, when the leak location is on the vertical and above-ground pipeline closer to the pump station, a relatively large leakage volumetric flow rate can be observed. The main reason is that the pressure inside the pipeline will be smaller as getting closer to the location of the pump station in the process of negative pressure extraction. A large pressure gradient between the roadway and the pipeline can be caused when an unexpected leakage occurs. Meanwhile, unlike the leak location on the underground pipeline, the variation of leakage volumetric flow rate in the case of vertical pipeline and above-ground pipeline shows an unstable trend over time. It may be because the strong mainstream inside the pipeline produces a great fluctuation near the leak location. In conclusion, a leak location closer to the pump station will generate a larger leakage volumetric flow rate. Therefore, it has a relatively big impact on the gas drainage process compared with leakage scenarios far away from the pump station.

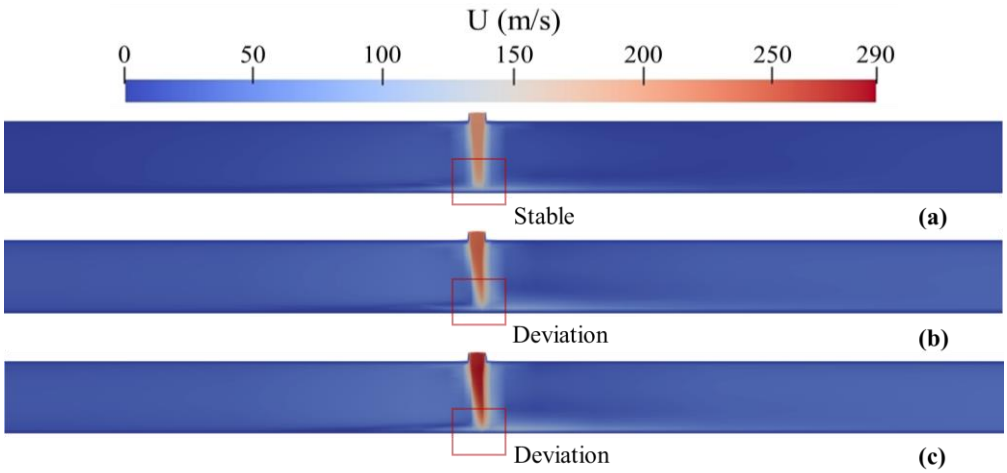

Fig. 13 Velocity contour of different leak locations, (a) Case 4: underground pipeline, (b) Case 5: vertical pipeline, (c) Case 6: above-ground pipeline.

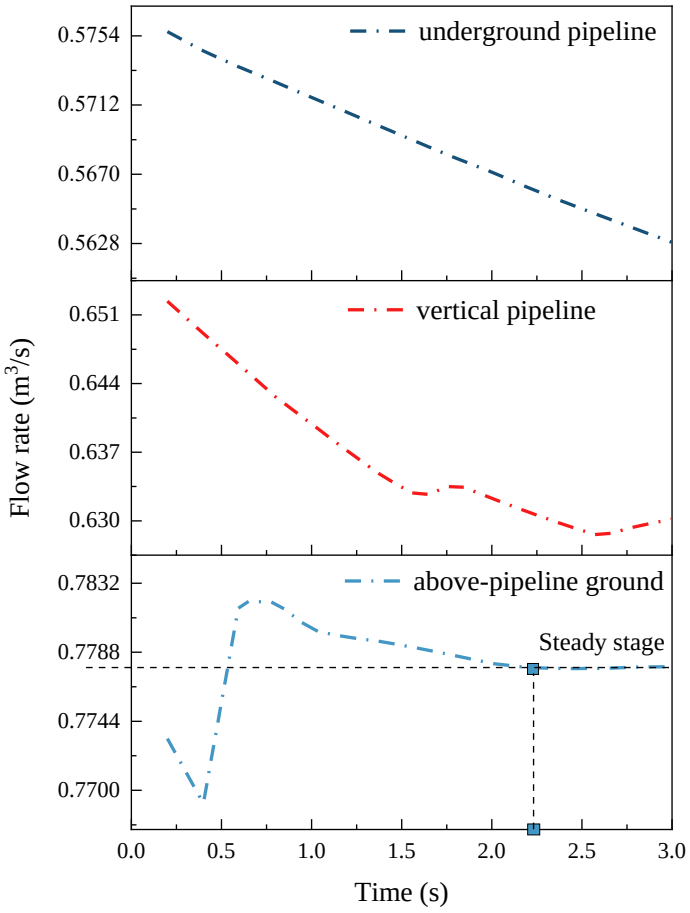

Fig. 14 Effect of leak locations on leakage flow rate.

Table 8 Velocity magnitude of the mainstream inside the pipeline

	Underground pipeline (Case 4: (-700,0,0))	Vertical pipeline (Case 5: (0,0,300))	Above-ground pipeline (Case 6: (100,0,600))
Velocity range (m/s)	9.62~10.23	31.97~37.25	37.81~39.24

Fig. 15 compares the CH4 concentration distribution of different leak locations. In the case of underground pipeline leakage, it shows a relatively obvious diffusion behavior both upstream and downstream of the leak location. While for the case of vertical and above-ground pipeline leakage, the variation of gas concentration is mainly distributed downstream of the leak location. Although leakage gas flow in the case of underground pipeline leakage can spread in two directions, a larger diffusion range can be obtained when the leak location is on the vertical and above-ground pipeline. Meanwhile, a relatively uniform CH4 concentration distribution can be observed. This is because the strong mainstream formed in the location close to the pump station prevents reverse flow. And the strong mainstream can accelerate the diffusion process of leakage gas flow to a large extent as well.

The relationship between CH4 concentration and leakage time is provided in Fig. 16 and Fig. 17. Fig. 16(a) indicates that CH4 concentration in the case of the leak location closer to the pump station (i.e., vertical pipeline and above-ground pipeline leakage) needs a shorter time to reach a relatively stable concentration (around 0.13VOL) and maintain a long duration within explosion limits. Therefore, these two cases represent high-risk leakage scenarios, especially a high-velocity mainstream existing inside the pipeline, which has a great probability of generating an electrostatic

spark. However, sensor 6 upstream of the leak location cannot capture the variation of gas concentration in the cases of vertical pipeline and above-pipeline leakage due to the strong mainstream inside the pipeline. Fig. 17 shows that the closer the leak location is to the pump station, the faster the gas concentration reaches the alarm threshold (0.77s, 0.15s, and 0.12s for the cases of underground pipeline, vertical pipeline, and above-ground pipeline leakage respectively). However, it can also be seen that all gas sensors located upstream of the leak location cannot detect the concentration variation effectively when the leak location is close to the pump station. All in all, a leakage consequence with a leak location close to the pump station usually has several characteristics: (1) large diffusion distance; (2) gas concentration within a dangerous range; (3) high gas velocity apt to cause the electrostatic spark; (4) invalid detection upstream of the leak location. Therefore, the location closer to the pump station should be allocated more resources for leakage detection and safety control.

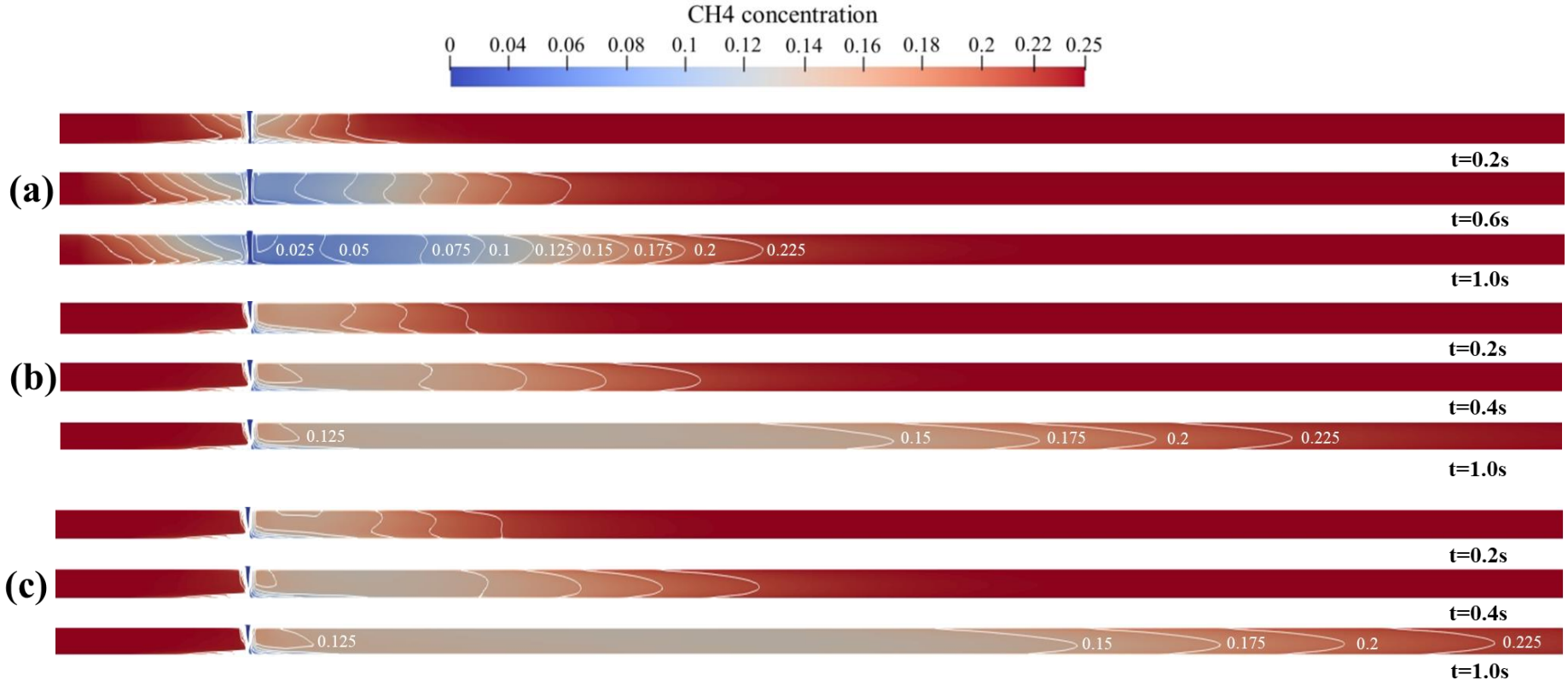

Fig. 15 CH4 concentration distribution of different leak locations, (a) Case 4: underground pipeline, (b) Case 5: vertical pipeline, (c) Case 6: above-ground pipeline.

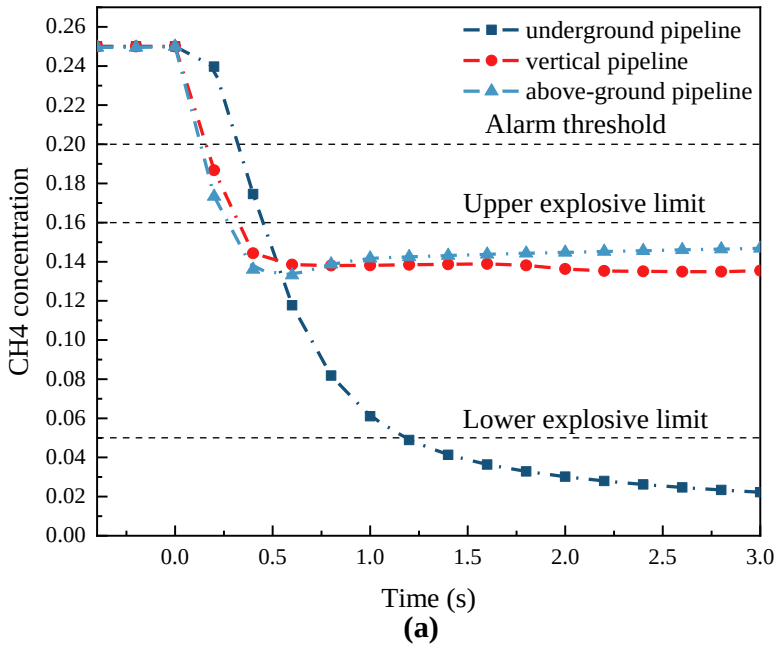

(a)

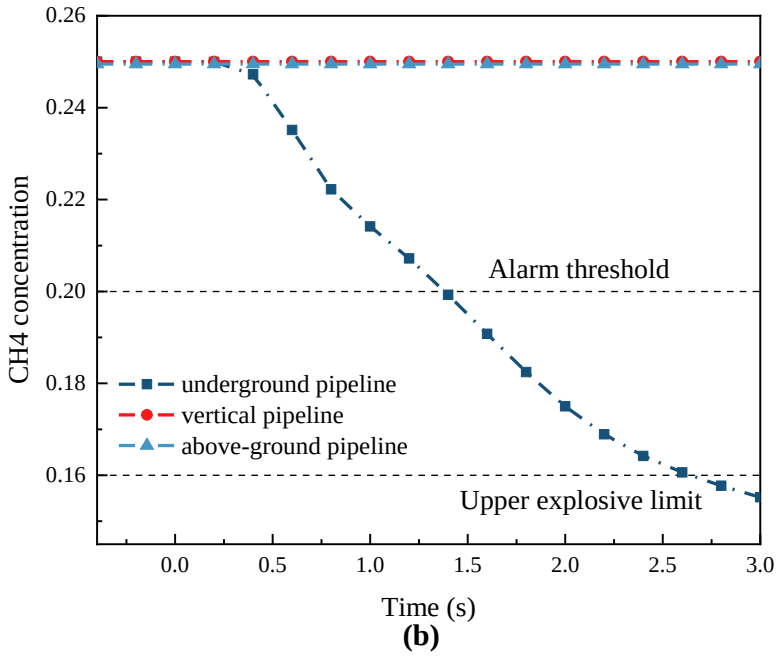

(b)

Fig. 16 Effect of different leak locations on alarm time, (a) sensor 1, (b) sensor 6.

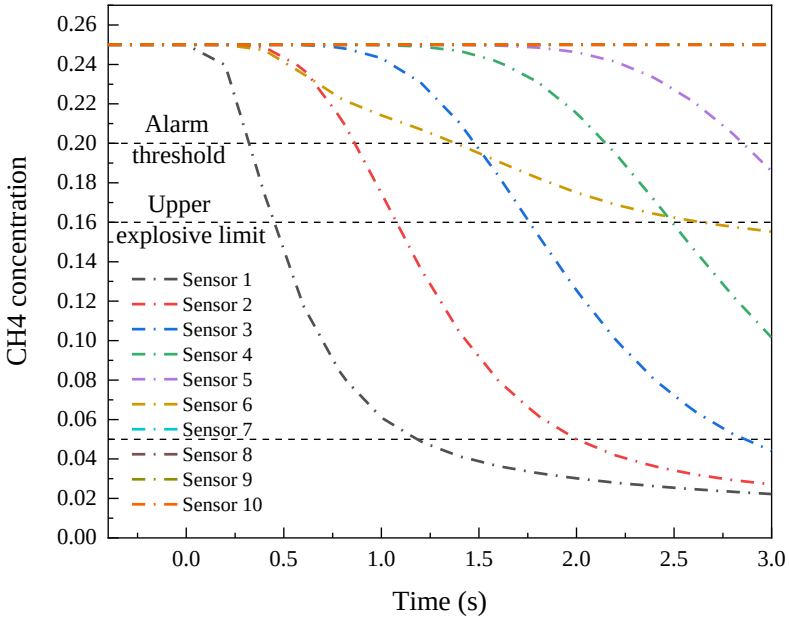
CH4 concentration
Time (s)
Alarm
threshold
Upper
explosive limit
Sensor 1
Sensor 2
Sensor 3
Sensor 4
Sensor 5
Sensor 6
Sensor 7
Sensor 8
Sensor 9
Sensor 10

(a)

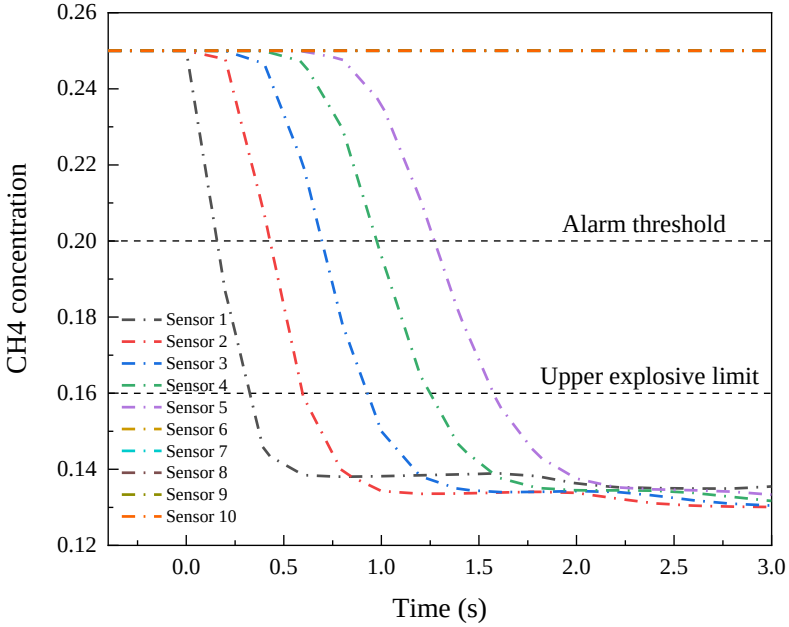
CH4 concentration
Time (s)
Alarm threshold
Upper explosive limit
Sensor 1
Sensor 2
Sensor 3
Sensor 4
Sensor 5
Sensor 6
Sensor 7
Sensor 8
Sensor 9
Sensor 10

(b)

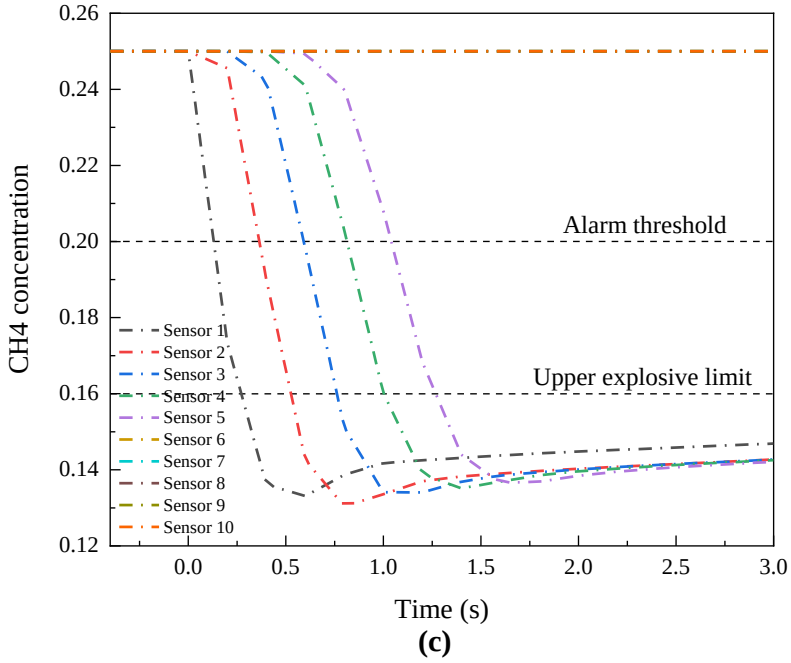

Fig. 17 Effect of different leak locations on alarm time, (a) Case 4: underground pipeline, (b) Case 5: vertical pipeline, (c) Case 6: above-ground pipeline.

3.2.4 Effects of pipeline diameters

In this section, the effects of different pipeline diameters (i.e., Case 7, Case 8, Case 9) on the process of gas leakage and diffusion are studied. The variation of velocity contour and leakage volumetric flow rate with different pipeline diameters are presented in Fig. 18 and Fig. 19. Fig. 18 shows that the leakage velocity increases with the increase of pipeline diameter. A slightly larger leakage volumetric flow rate will be obtained with a larger pipeline diameter and thus have a greater negative impact on the quality of extracted gas, which can be seen in Fig. 19. This may be because a large high-pressure area is generated in the lower part of the pipeline for a small pipeline diameter since the leakage gas flow impinges on the pipeline wall. Subject to the large high-

pressure area, there is a great change of pressure gradient near the leak location, which makes the pressure gradient normal to the leakage hole small but unstable. Likewise, this is why the variation of RVR over time is large in the case of small pipeline diameter.

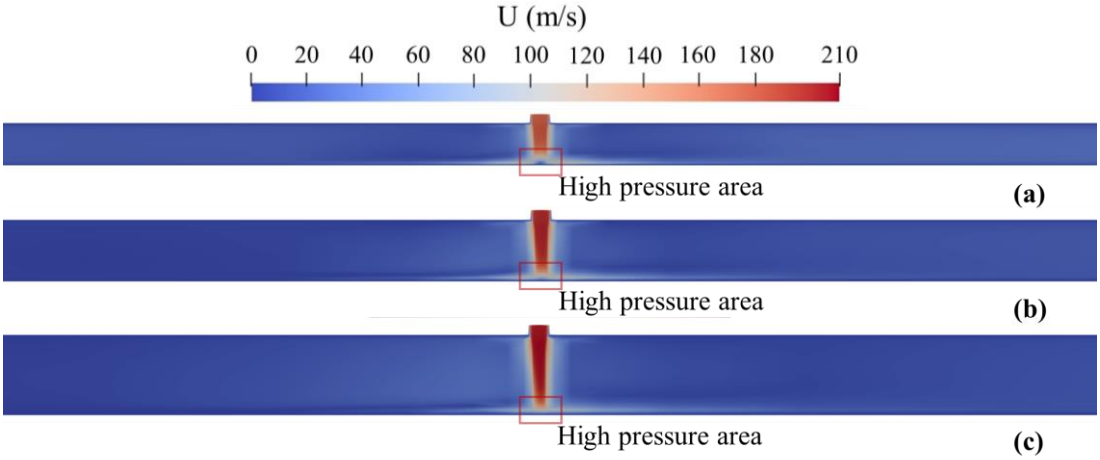

Fig. 18 Velocity contour of different pipeline diameters, (a) Case 7: 426mm, (b) Case 8: 630mm, (c) Case 9: 820mm.

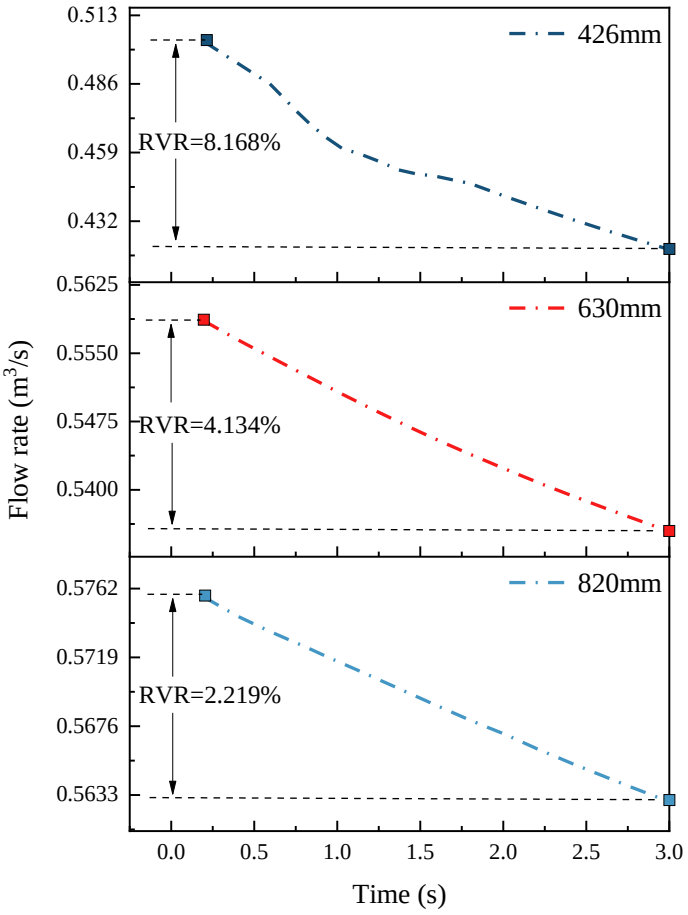

Fig. 19 Effect of different pipeline diameters on leakage flow rate.

Fig. 20 presents the CH4 concentration contours under different pipeline diameters. With the decrease of the pipeline diameter, there is a more obvious bidirectional diffusion behavior and the low-concentration region becomes larger. Fig. 20 shows that the region influenced by leakage accident in the case of 426mm, 630mm, and 820mm at t=1s is 109m, 77m, and 54m respectively. This can be attributed to the limited space inside the pipeline and the large high-pressure area at the leakage location for the case of small pipeline diameter. Therefore, when it comes to the case of a smaller pipeline diameter, the leakage gas flow can overcome the influence of the mainstream and thus spread both downstream and upstream for a long distance.

As shown in Fig. 21(a), it can be seen that the alarm time will be shorter as the pipeline diameter become smaller. Fig. 21(b) indicates that the different pipeline diameters have a critical role in alarm time (0.16s, 0.46s, and 1.40s for the case of 426mm, 630mm, 820mm respectively) for gas sensor located upstream of the leak location. Fig. 22 shows that a smaller pipeline diameter will extremely affect the gas concentration downstream and upstream in the aspect of influence region and alarm time. It means that a smaller pipeline will suppress the CH4 concentration to a very low level in a short time, which cause a great waste of gas resources and potentially hazardous condition.

In this study, all gas sensors can be triggered in the case of 426mm according to the alarm threshold (0.2VOL). Therefore, the alarm time in the case of 426mm is extracted and fitted to study the relationship between alarm time and location along the pipeline. As can be seen from Fig. 23, the alarm time for both gas sensors distributed upstream and downstream is second-order relation of distance away from the leak location. Meanwhile, the farther the distance away from the leak location, the greater the difference of alarm time between gas sensors distributed upstream and downstream at the symmetrical location. This is because the effect of the mainstream on the leakage gas flow increases with a farther distance away from the leak location. which performs as a resistance preventing the upstream reverse flow inside the pipeline. This relationship can provide some reference for the monitoring system design.

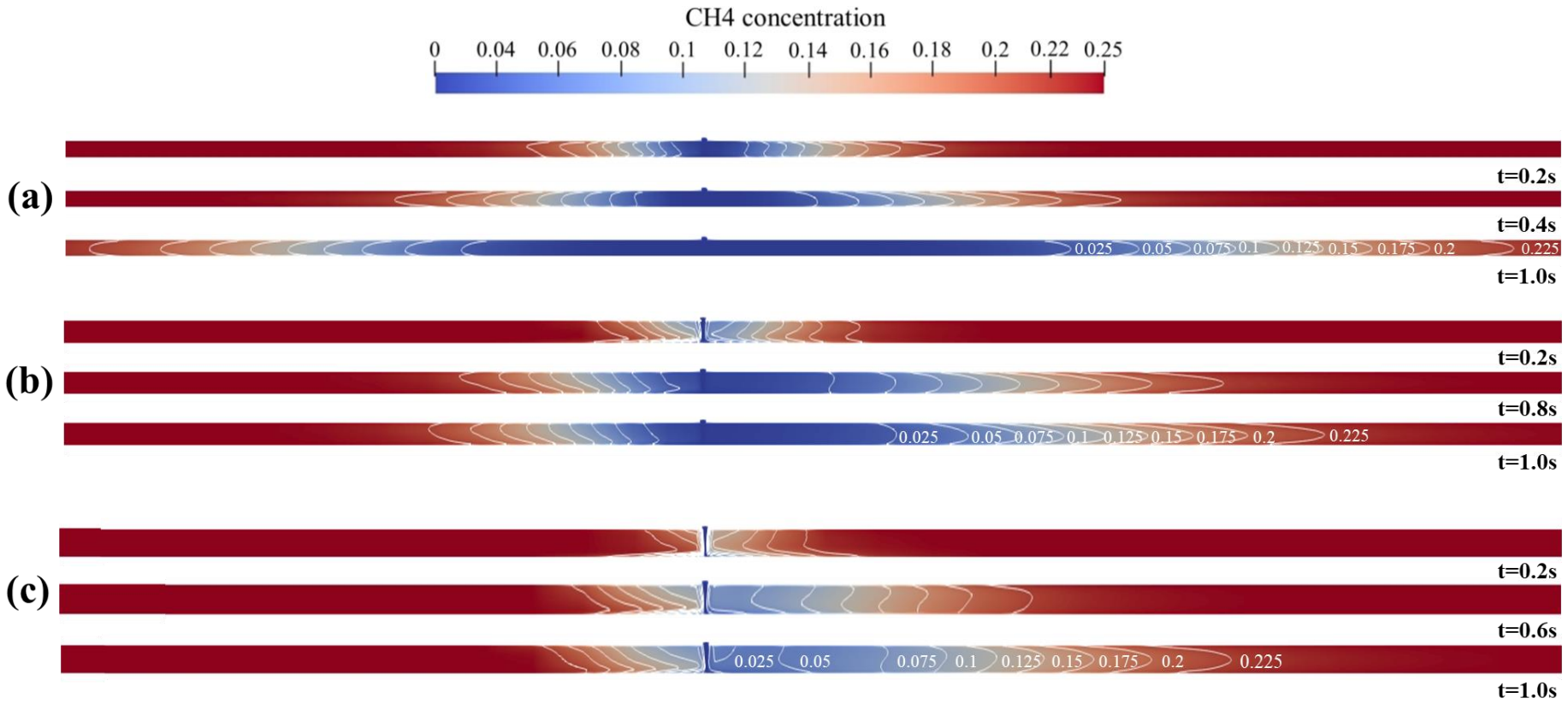

Fig. 20 CH4 concentration distribution of different pipeline diameters, (a) Case 7: 426mm, (b) Case 8: 630mm, (c) Case 9: 820mm.

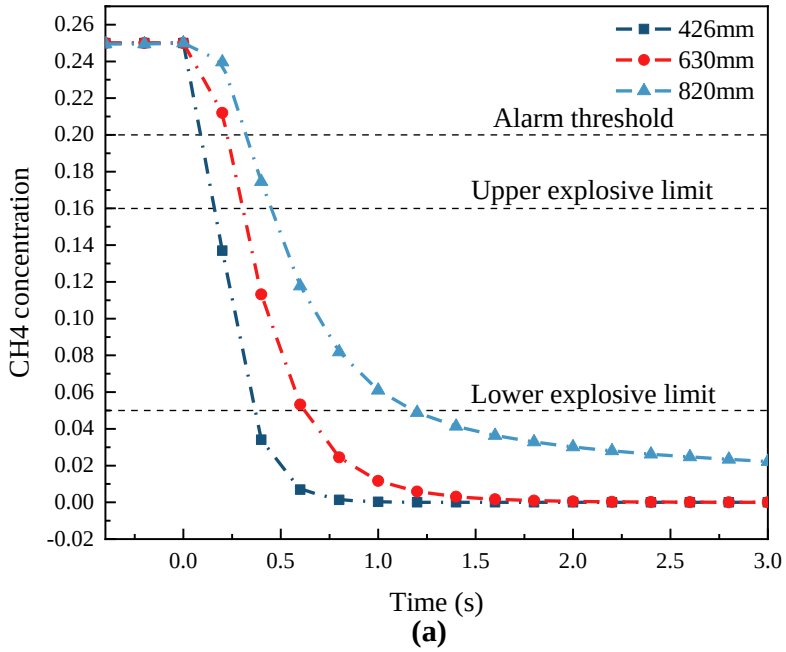

(a)

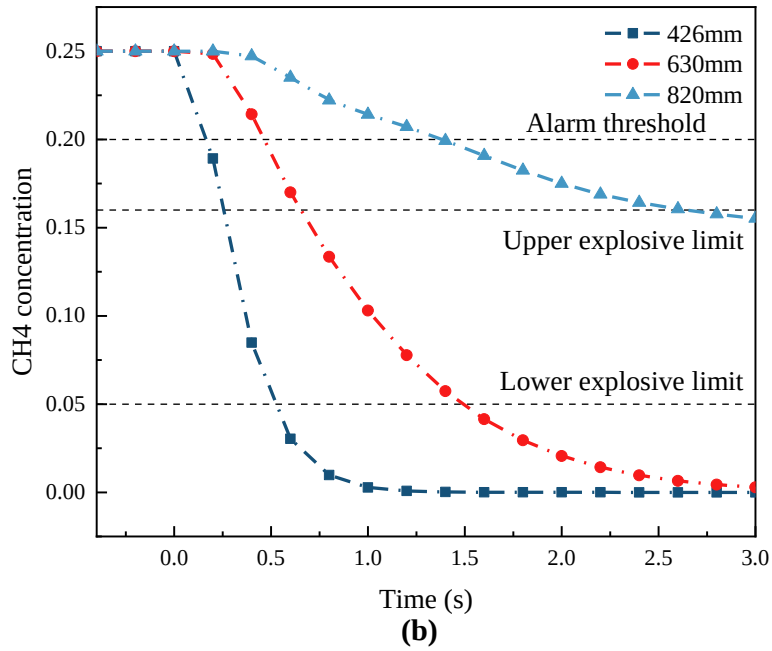

(b)

Fig. 21 Effect of different pipeline diameters on alarm time, (a) sensor 1, (b) sensor 6.

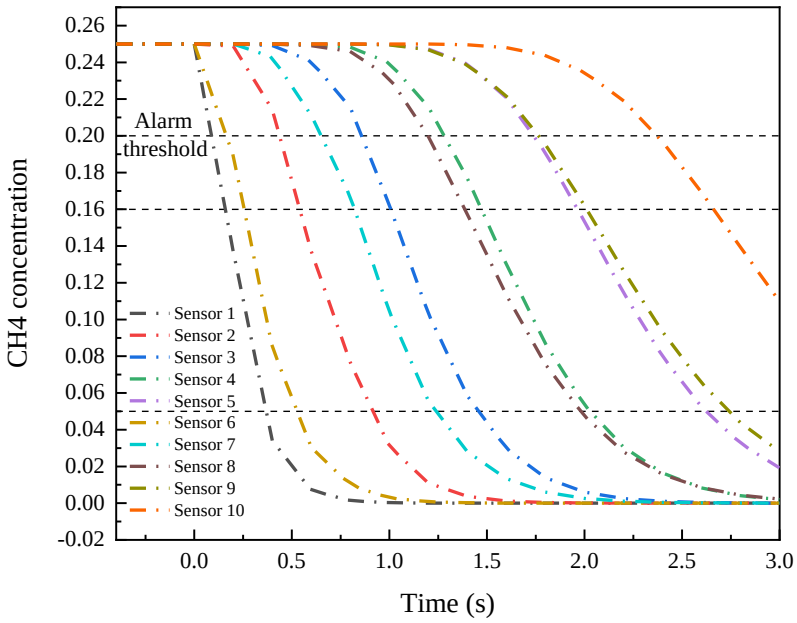
CH4 concentration
Time (s)
Alarm
threshold
Sensor 1
Sensor 2
Sensor 3
Sensor 4
Sensor 5
Sensor 6
Sensor 7
Sensor 8
Sensor 9
Sensor 10
0.26
0.24
0.22
0.20
0.18
0.16
0.14
0.12
0.10
0.08
0.06
0.04
0.02
0.00
-0.02
0.0
0.5
1.0
1.5
2.0
2.5
3.0

(a)

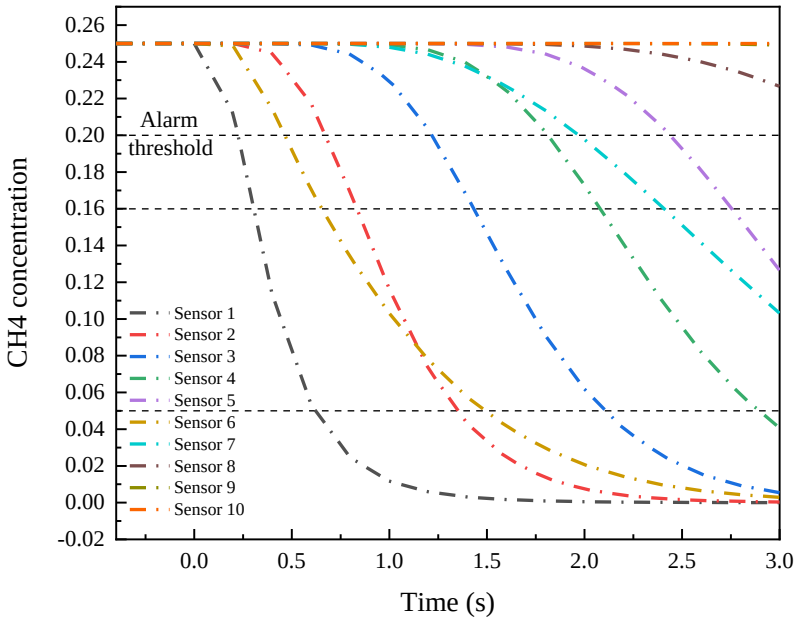
CH4 concentration
Time (s)
Alarm
threshold
Sensor 1
Sensor 2
Sensor 3
Sensor 4
Sensor 5
Sensor 6
Sensor 7
Sensor 8
Sensor 9
Sensor 10
0.26
0.24
0.22
0.20
0.18
0.16
0.14
0.12
0.10
0.08
0.06
0.04
0.02
0.00
-0.02
0.0
0.5
1.0
1.5
2.0
2.5
3.0

(b)

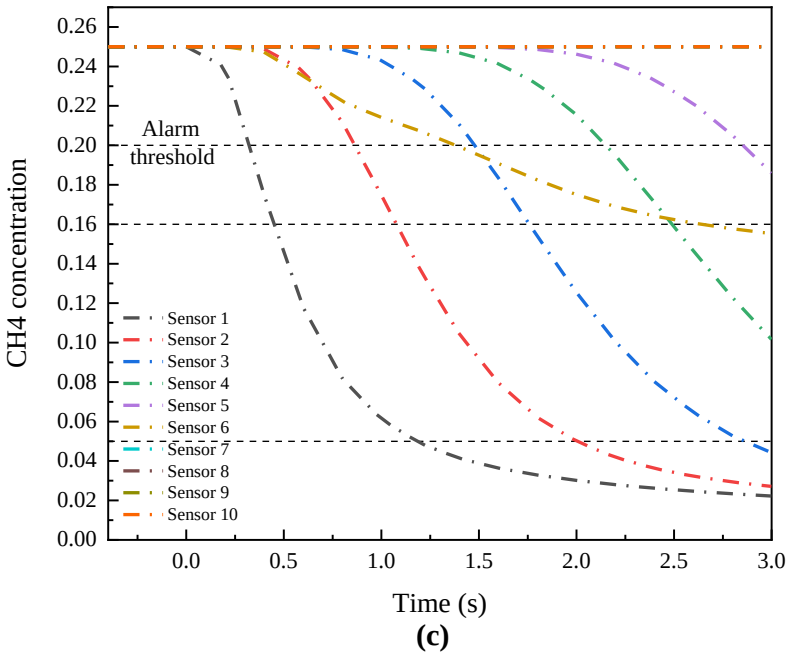

Fig. 22 Effect of different pipeline diameters on alarm time, (a) Case 7: 426mm, (b) Case 8: 630mm, (c) Case 9: 820mm.

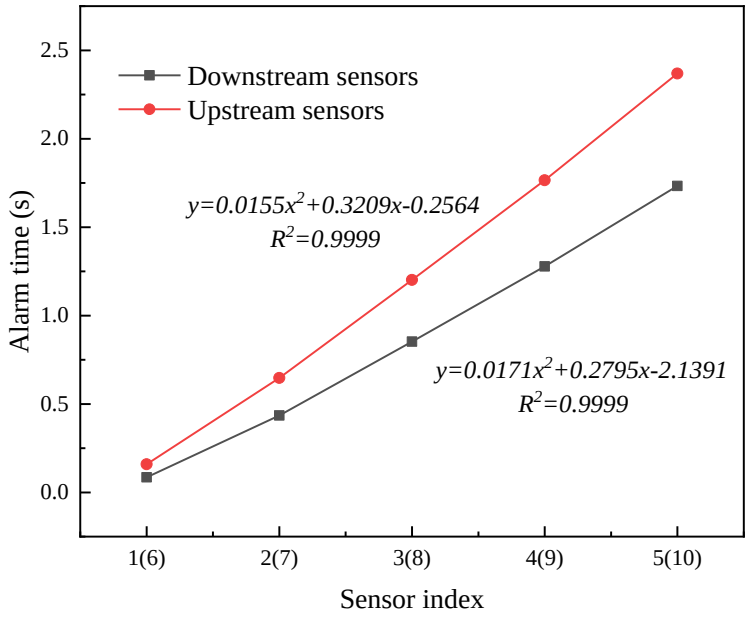

Fig. 23 Relationship between alarm time and the location of gas sensors (Case 7: 426mm).

4. Conclusion

This study proposed a multi-factors gas drainage pipeline leakage and diffusion (GDPLD) model based on the OpenFOAM platform. The feasibility and practicality of

the proposed model were evaluated through field measurement data. The multi-factors scenario analysis was conducted to investigate the leakage and diffusion characteristics of the gas drainage pipeline in the underground coal mine. The main conclusions of this study are summarized as follows:

(1) The GDPLD model was developed and verified through an empirical formula in a previous study and field measurement data. The results showed that the proposed model can well reproduce the leakage and diffusion behaviors of gas drainage pipelines with a 4.3% max relative error.

(2) In multi-factors scenario analysis, the variation of leak sizes, leak locations, and pipeline diameters mainly affect the leakage volumetric flow rate (0.03, 0.56, and 2.69 m^3/s for three leak size cases), downstream gas velocity (10.23, 37.25, and 39.24m/s for three leak location cases), and internal space of the pipeline (the cross-sectional areas of the three pipeline diameter cases are 0.14, 0.31, and 0.52m^2). Therefore, these three factors can affect the leakage volumetric flow rate, gas concentration distribution, and alarm time of observation sensors in varying degrees.

(3) The detection of pipeline leakage will be influenced by the leakage volumetric flow rate, the confined space inside the pipeline, and the mainstream inside the pipeline, which are dominated by leak size, pipeline diameter, and leak location respectively. By

considering the shortest alarm time and the number of triggered sensors (0.2s, 0.12s, 0.15s for the leak size, leak location, and pipeline diameter scenarios respectively; 8, 6, 10 for these three scenarios), the influence factor of pipeline diameters performs a more obvious impact on the detection of pipeline leakage.

Acknowledgements

This work was supported by the National Key Research and Development Program of China (Grant No. 2017YFC0805001) and the Yue Qi Young Scholar Program of China University of Mining & Technology, Beijing.

Appendix A.

Table A1 Parameter of the SST model

Turbulence Model	F_1	β^*	β	σ_k	σ_ω
k-ε	0	0.09	3/40	0.85	0.5
k-ω	1	0.09	0.0828	1	0.856

Table A2 Configurations parameters of the gas drainage pipeline model

Parameter	value
Length of 820 mm diameter pipeline (m)	3755
Length of 630 mm diameter pipeline (m)	2067
Length of 426 mm diameter pipeline (m)	776
Environment average temperature (K)	290.54
Average concentration of extracted gas (%)	20

References

Anselmet, F., Ternat, F., Amielh, M., Boiron, O., Boyer, P., Pietri, L., 2009. Axial development of the mean flow in the entrance region of turbulent pipe and duct

flows. C. R. Mecanique. 337, 573-584.

Bezaatpour, J., Fatehifar, E., Rasoulzadeh, A., 2020. CFD investigation of natural gas leakage and propagation from buried pipeline for anisotropic and partially saturated multilayer soil. Journal of Cleaner Production. 277, 123940.

Cao, J., Dai, L., Sun, H., Wang, B., Zhao, B., Yang, X., Zhao, X., Guo, P., 2019. Experimental study of the impact of gas adsorption on coal and gas outburst dynamic effects. Process Safety and Environmental Protection. 128, 158-166.

Cheng, Y., Dong, J., Li, W., Chen, M., Liu, K., 2017. Effect of negative pressure on coalbed methane extraction and application in the utilization of methane resource. Journal of China Coal Society. 42(6), 1466-1474.

Ebrahimi-Moghadam, A., Farzaneh-Gord, M., Deymi-Dashtebayaz, M., 2016. Correlations for estimating natural gas leakage from above-ground and buried urban distribution pipelines. Journal of Natural Gas Science and Engineering. 34, 185-196.

Ebrahimi-Moghadam, A., Farzaneh-Gord, M., Arabkoohsar, A., Jabari Moghadam, A., 2018. CFD analysis of natural gas emission from damaged pipelines: Correlation development for leakage estimation. Journal of Cleaner Production. 199, 257-271.

Fan, J., Liu, P., Li, J., Jiang, D., 2020. A coupled methane/air flow model for coal gas drainage : Model development and finite-difference solution. Process Safety and Environmental Protection. 141, 288–304.

Fiates J., Vianna S., 2016. Numerical modelling of gas dispersion using OpenFOAM. Process Safety and Environmental Protection. 104, 277-293.

Kang, J., Zhou, F., Qiang, Z., Zhu, S., 2018. Evaluation of gas drainage and coal permeability improvement with liquid CO2 gasification blasting. Advances in Mechanical Engineering. 10(4), 1-15.

Liu, A., Liu, S., Hou, X., Liu, P., 2020. Transient gas diffusivity evaluation and modeling for methane and helium in coal. International Journal of Heat and Mass Transfer. 159, 120091.

Liu, H., Ding, W., Zhou, F., Yang, G., Du, Y., 2020. An overview and outlook on gas adsorption: for the enrichment of low concentration coalbed methane. Separation Science and Technology. 55(6), 1102-1114.

Liu, P., Fan, J., Jiang, D., Li, J., 2021. Evaluation of underground coal gas drainage performance: Mine site measurements and parametric sensitivity analysis. Process Safety and Environmental Protection. 148, 711-723.

Liu, P., Jiang, Y., Fu, B., 2020. A novel approach to characterize gas flow behaviors and air leakage mechanisms in fracture-matrix coal around in-seam drainage borehole. Journal of Natural Gas Science and Engineering. 77, 103243.

Liu, T., Lin, B., Fu, X., Zhu, C., 2020. Modeling air leakage around gas extraction boreholes in mining-disturbed coal seams. Process Safety and Environmental Protection. 141, 202-214.

Lu, S., Wang, C., Liu, Q., Zhang, Y., Liu, J., Sa, Z., Wang, L., 2019. Numerical assessment of the energy instability of gas outburst of deformed and normal coal combinations during mining. Process Safety and Environmental Protection. 132, 351-366.

Mack, A., Spruijt, M., 2013. Validation of OpenFoam for heavy gas dispersion applications. Journal of Hazardous Materials. 262, 504-516.

Menter, F., 1994. Two-Equation Eddy-Viscosity Turbulence Models for Engineering Applications. AIAA Journal. 32, 1598-1605.

Menter, F., Kuntz, M., Langtry, R., 2003. Ten years of industrial experience with the

SST turbulence model. Proceedings of the fourth international symposium on Turbulence. Heat and Mass Transfer, 625–632.

Moore T., 2012. Coalbed methane: A review. International Journal of Coal Geology. 101, 36–81.

Okamoto, H., Gomi, Y., 2011. Empirical research on diffusion behavior of leaked gas in the ground. Journal of Loss Prevention in the Process Industries. 24, 531-540.

Park, S., Liang, Y., 2016. Biogenic methane production from coal: A review on recent research and development on microbially enhanced coalbed methane (MECBM). Fuel. 166, 258–267.

Peng, S., Zhang C., Liang Y., Xu, J., Liu, D., 2015. Physical simulation experiment on the evolution of gas pressure during CBM drainage. Journal of China Coal Society. 40(3), 571-578.

Sklavounos, S., Rigas, F., 2004. Validation of turbulence models in heavy gas dispersion over obstacles. Journal of Hazardous Materials. A108, 9-20.

Tran, V., Ng, E., Skote, M. CFD simulation of dense gas dispersion in neutral atmospheric boundary layer with OpenFOAM. Meteorology and Atmospheric Physics. 132, 273-285.

Wang, C., Yang, S., Li, X., 2018. Simulation of the hazard arising from the coupling of gas explosions and spontaneously combustible coal due to the gas drainage of a gob. Process Safety and Environmental Protection. 118, 296-306.

Wang, H., Wang, E., Li, Z., Wang, X., Zhang, Q., Li, B., Ali, M., 2020. Study on sealing effect of pre-drainage gas borehole in coal seam based on air-gas mixed flow coupling model. Process Safety and Environmental Protection. 136, 15-27.

Wang, K., Lou, Z., Wei, G., Qin, B., Wang, L., 2019. A novel anti-air-leakage method

and an organic polymer material for improving methane drainage performance. Process Safety and Environmental Protection. 129, 152-162.

Wang, X., Tan, Y., Zhang, T., Zhang, J., Yu, K., 2020. Diffusion process simulation and ventilation strategy for small-hole natural gas leakage in utility tunnels. Tunnelling and Underground Space Technology. 97, 103276.

Wang, X., Zhou, F., Xia, T., Xu, M., 2016. A multi-objective optimization model to enhance the comprehensive performance of underground gas drainage system. Journal of Natural Gas Science and Engineering. 36, 852-864.

Wang, Z., Sun, Y., Wang, Y., Zhang, J., Sun, Z., 2019. A coupled model of air leakage in gas drainage and an active support sealing method for improving drainage performance. Fuel. 237, 1217-1227.

Yan, Y., Dong, X., Li, J., 2015. Experimental study of methane diffusion in soil for an underground gas pipe leak. Journal of Natural Gas Science and Engineering. 27, 82-89.

Zhang, J., Li, B., Sun, Y., 2018. Dynamic leakage mechanism of gas drainage borehole and engineering application. International Journal of Mining Science and Technology. 28, 505-512.

Zhang, P., Lan, H., 2020. Effects of ventilation on leakage and diffusion law of gas pipeline in utility tunnel. Tunnelling and Underground Space Technology. 105, 103557.

Zhang, X., Su, G., Chen, J., Raskob, W., Yuan, H., Huang, Q., 2015. Iterative ensemble Kalman filter for atmospheric dispersion in nuclear accidents: An application to Kincaid tracer experiment. Journal of Hazardous Materials. 297, 329-339.

Zhang, X., Su, G., Yuan, H., Chen, J., Huang, Q., 2014. Modified ensemble Kalman

filter for nuclear accident atmospheric dispersion: Prediction improved and source estimated. Journal of Hazardous Materials. 280, 143-155.

Zhang, Y., Hu, S., Xia, T., Liu, Y., Pan, Z., Zhou, F., 2020. A novel failure control technology of cross-measure borehole for gas drainage: A case study. Process Safety and Environmental Protection. 135, 144-156

Zhang, Y., Zou, Q., Guo, L., 2020. Air-leakage Model and Sealing Technique with Sealing–Isolation Integration for Gas-drainage Boreholes in Coal Mines. Process Safety and Environmental Protection. 140, 258-272.

Zhao, D., Liu, J., Pan, J. T., 2018. Study on gas seepage from coal seams in the distance between boreholes for gas extraction. Journal of Loss Prevention in the Process Industries. 54, 266-272.

Zheng C., Jiang B., Xue, S., Chen, Z., Li, H., 2019. Coalbed methane emissions and drainage methods in underground mining for mining safety and environmental benefits: A review. Process Safety and Environmental Protection. 127, 103-124.

Zheng, C., Chen, Z., Kizil, M., Aminossadati, S., Zou, Q., Gao, P., 2016. Characterisation of mechanics and flow fields around in-seam methane gas drainage borehole for preventing ventilation air leakage: A case study. International Journal of Coal Geology. 162, 123-138.

Zheng, C., Kizil, M., Chen, Z., Aminossadati, S., 2017. Effects of coal properties on ventilation air leakage into methane gas drainage boreholes: Application of the orthogonal design. Journal of Natural Gas Science and Engineering. 45, 88-95.

Zhou, A., Zhang, M., Wang, K., Zhang, X., Feng, T., 2020. Quantitative study on gas dynamic characteristics of two-phase gas-solid flow in coal and gas outbursts. Process Safety and Environmental Protection. 139, 251-261.

Zhou, F., Wang, X., Xia, T., 2014. A model of safe drainage of coal seam gas. Journal of China Coal Society. 39(8), 1659-1666.